Final Degree Thesis

A Feasibility Study of the Suitability of an AD5933-based Spectrometer for EBI Applications

By

Antonio Ansede Pena

UNIVERSITY OF BORÅS

SCHOOL OF ENGINEERING

FINAL DEGREE THESIS 30 ECTS, ERASMUS 2009-10 SWEDEN
ELECTRICAL ENGINEERING SPECIALIZATION IN COMMUNICATIONS & SIGNAL PROCESSING
THESIS Nº9/2009

A Feasibility Study of the Suitability of an AD5933-based Spectrometer for EBI Applications

Antonio Ansede Pena

Final Degree Thesis

Subject Category: Medical Technology, Electronic Instrumentation

University of Borås

School of Engineering

SE- 501 90 BORAS

Telephone +46 33 435 4640

Examiner: Fernando Seoane Martínez

Supervisor: Fernando Seoane Martínez

Date: 2009 Sept 28th

Keyword: Electrical Bioimpedance, Electrical Bioimpedance Spectroscopy, AD5933, SFB7, Analog Frond End, Statistical Analysis, Wearable Medical Devices.

ABSTRACT

Electrical Bioimpedance (EBI) measurements have proven their validity in several medical applications like body composition analysis and detection of melanoma among others. The successful application of EBI technology on the field of medicine has lead the way for applications in the field of personal healthcare and body performance in the field of sports.

Due to the widespread use of the EBI technology and rising of new EBI applications requiring system portability or even suitable to wear, the manufacturer Analog devices has introduced in the market the first integrated system dedicated to measure EBI, the impedance network analyzer AD5933. The availability of this EBI spectrometer device opens up new horizons for the integration of the measurement systems to meet the demands of new EBI applications and allowing the development of portable and even wearable measurement systems.

This project is focused on the AD5933 impedance network analyzer, and it aims to identify the EBI applications in which, the use of an AD5933 device is suitable. To adapt the AD5933 device for biomedical measurements an Analog Front-End (AFE) has been used to enable the system for 4-electrodes measurements. In order to evaluate the performance of AD5933 with the AFE, experimental measurements on electrical equivalent models have been taken with the AD5933+4E-AFE system and the EBI spectrometer Impedimed SFB7. The obtained impedance spectral data have been used to estimate the values of the equivalent circuit under measurement and the estimated values have been mutually compared in terms of estimation accuracy.

ACKNOWLEDGEMENTS

First I would like to thank specially my thesis supervisor, Dr. Fernando Seoane, for his encouragement and patience throughout the duration of this final degree thesis and I would like to specifically appreciate all the dedication that he has provided me. Fernando, I am deeply thankful for all the knowledge that you have shared with me and for all the good moments.

I am also grateful to my colleagues and friends, David A., Ivan Pau, Javier F., Juan Carlos M., Lola R., Rubén B., Ruth G., Ruth P. for his helpful comments and ideas and for made more enjoyable to work at the BRC (Bioimpedance Research Center) and for the great moments together.

I would like to thank to the Polytechnic University of Catalonia for giving me the opportunity to come to Borås and especially to Prof. Pere Joan Riu Costa, Dr. Ramon Bragós Bardia and Dr. Lluís Prat Viñas.

And above all I want to thanks to my friends and family, my mother Maria del Carmen, my girlfriend Diana, my uncles Suso and Modesto, my aunts Elvira and Blanca, my grandparents Antonio and Efigenia and my cousins Elvi and Maria Jesus, for giving me always support and to encourage me whenever I needed it. I dedicate this work to all of you.

Antonio Ansede

TABLE OF CONTENTS

LIST OF ACRONYMS

AA	-	Arm-Arm
ADC	-	Analog Digital Converter
AFE	-	Analog Front End
BCM	-	Body Cell Mass
BIA	-	Bioimpedance Analysis
BIS	-	Bioimpedance Spectroscopy
BIVA	-	Bioimpedance Vector Analysis
DSP	-	Digital Signal Processor
EBI	-	Electrical Bioimpedance
ECW	-	Extra Cellular Water
FC	-	Characteristic Frequency
FFM	-	Fat Free Mass
LC	-	Lungs Composition
LL	-	Leg-Leg
MF-BIA	-	Multi Frequency Bioimpedance Analysis
RR	-	Respiration Rate
SBC	-	Segmental Body Composition
SF-BIA	-	Single Frequency Bioimpedance Analysis
TBW	-	Total Body Water
TT	-	Trunk- Trunk
ICG	-	Impedance CardioGraphy
ICF	-	IntraCellular Fluid

CHAPTER 1

INTRODUCTION

1.1 Introduction

Nowadays there is many and several applications of Electrical Bioimpedance (EBI), these have been emerging as answers to clinical needs as methods for non-invasive monitoring and the detection of changes in the structure and composition of tissues produced by pathophysiological processes.

A new Integrated Circuit (IC), the AD5933 is available to perform EBI measurements allowing for the development of small-integrated EBI measurement systems enabling portable and wearable systems.

1.2. Motivation

The increase of ageing population demands that the model of hospital centered healthcare turns towards one model of healthcare more personalized and home care-based. In this way, the patient involvement on the health care process will increase potentially increasing prevention and early detection what will provide eventually in a better and more affordable treatment. Such changes create the need to develop a new efficient, sustainable and useful technology to equip the patient with a tool for a personal health monitoring and simultaneously allowing the healthcare staff to monitor remotely the conditions of the patients.

The latter together with the technological development of the field of functional textiles point out to the emerging area of personalized healthcare monitoring as plausible area of operation. EBI technology combines both the potential to be used in personalized healthcare as well as being able to benefit from the technological developments within functional textiles. The only piece missing to enable the development of wearable EBI measurement systems for personalized healthcare monitoring is the electronic device that will allow the implementation of EBI measurement systems as wearable systems.

Recently the manufacturer of integrated circuits, Analog Devices, has introduced in the market the first integrated system dedicated to measure EBI: the AD5933. The availability of this EBI spectrometer device opens up new horizons for the integration of the measurement systems of EBI into portable and even wearable systems. To adapt the AD5933 device for human measurements an Analog Front-End has been developed to realize measurements with four electrodes wires.

There are many applications that could benefit from such a small device the AD5933 and a natural and mandatory step in any development process is to identify which medical and

healthcare applications of EBI are potential candidates to benefit from the use AD5933-based systems.

1.3. Goal

The main goal of this thesis is to identify the EBI applications suitable to be implemented with an AD5933 enabled system.

1.4. Work done

As previously mentioned, this project is focused on the identification of applications of EBI suitable to be implemented with the set AD5933 + 4E-AFE. In order to reach the mentioned goal, the following work has been done:

- Experimental EBI Measurements have been taken with the device SFB7 in a healthy subject for the following EBI applications:
  - Total Body Composition (TBC)
  - Respiration Rate (RR)
  - Lungs Composition (LC)
  - Segmental Body Composition (SBC)
    - Arm-Arm (AA)
    - Leg-Leg (LL)
    - Trunk-Trunk (TT)
- Experimentally based electrical 2R1C models equivalent to each EBI application have been built.
- The AD5933+4E-AFE has been customized by adjusting the values of internal components to each of the applications.
- For comparison purposes Impedance measurements on each of the built 2R1C model have been performed with both the AD5933+4E-AFE device and the SFB7 Spectrometer.
- All the obtained measurements, from both spectrometers, have been processed and a performance comparison has been done based on the bias error obtained on the estimation of the value of the original model parameters.

1.5. Structure of the Thesis Report

This thesis report is organized in 6 chapters and a final section for the references. Chapter 1 contains the introduction part of this thesis report. Chapter 2 provides a brief background EBI, the measurement methods and the applications. Chapter 3 describes the instrumentation and the methods used in this thesis while Chapter 4 shows the obtained results. Finally, Chapter 5

discusses the results and the work done and Chapter 6 ends the report with the conclusion and proposal for future work.

1.6. Out of Scope

The following issues have not covered during this thesis work because they have been considerate outside the scope of the project:

- To implement a new embedded system and software with the purpose to implement an automatic customization of the AD5933 +4F-AFE.

- To test for the plausibility of EBI applications those require short time-continuous measurements like impedance cardiography (ICG).

CHAPTER 2

BACKGROUND

2.1. Introduction to Electrical Bioimpedance

2.1.1. Historical Introduction

The first reported contact with the electrical properties of biological tissue was done by Luigi Galvani [1], who on 1780 observed that while an assistant was touching the sciatic nerve of a frog with a metal scalpel, the frog's muscle moved when he drew electric arcs on a nearby electrostatic machine.

After several developments in electronic instrumentation like the Volta electrochemical battery as the Continuous DC current source developed by Volta in 1800, the galvanometer from 1820, high AC voltage/current pulse generators from 1831 and the continuous AC current sources from 1867, the detection of small bioelectrical currents became possible.

It was not until 1921 that Phillippson [4] made the first tissue impedance measurement as a function of frequency, and found that the capacitance varied approximately as the inverse square root of the frequency. After that, Fricke in 1924 [5] proposed an electrical equivalent model of Bioimpedance for tissue and blood, here he assumed that cell are electrically represented by a resistance *Ri,* intracellular fluid and capacitance *C,* cell membrane, in series and a resistance *Re* representing the extracellular fluid in parallel. In 1928, 4 years before the publication of Fricke, Kenneth S. Cole [6] found the expressions for the impedance at DC and infinite frequency and paved the way for an analytical and mathematical treatment of tissue immittivity and permittivity.

Therefore, the first application of bioimpedance techniques for monitoring applications appeared as early as 1940, impedance cardiography [7]. Since then, bioimpedance measurements have been used in several medical applications; examples from a long list are lung function monitoring [8], body composition [9] and skin cancer detection [10].

2.1.2. Electricals Properties of Biological Tissue

The passive electrical properties, conductivity and permittivity, of biological tissue have their origin on the biochemical and structural composition of biological tissue. The uneven distribution of the body constituents and the morphological differences among cells confer to most of tissues with a high grade of anisotropy and inhomogeneity of their electrical properties.

TABLE 2.1: CONCENTRATION OF ELECTROLYTES IN BODY LIQUIDS (MEQ/L)

IS ION. CONCENTRATION IN MILLIEQUIVALENTS (MMOLE*VALENCY Z) PER LITER.

Cations (meq/L)			Anions (meq/L)		
	Plasma	Intracellular		Plasma	Intracellular
Na^+	142	10	Cl^-	103	4
K^+	4	140	HCO_3^-	24	10
Ca^{2+}	5	10^{-4}	$Protein^-$	16	36
Mg^{2+}	2	30	$HPO_4^{2-} + SO_4^{2-}$ + organic acids	10	130
H^+ (pH = 7.4)	4×10^{-5}	4×10^{-5}			
Sum	153	180	Sum	153	180

0.9% NaCl is 154 mmol/L.

Note. Table extracted from [1]

Most often biological tissues are composed by group of cells, which are surrounded by a cell membrane containing the intracellular fluid inside the cell membrane, that are suspended on extracellular fluid. Both intracellular and extracellular fluids are rich in proteins and electrolytes, see Table 2.1 Such composition provides them with ionic conductivity and are often modeled, from an electrical point of view, as a conductance.

One of the most important constituents of the cell is the plasmatic membrane, also known as cell membrane. The cell membrane is a layer that separates two different physiological spaces. The cell membrane consists of proteins and phospholipids forming a bilayer lipid membrane of approximately 7 nm thick. See Figure 2.1

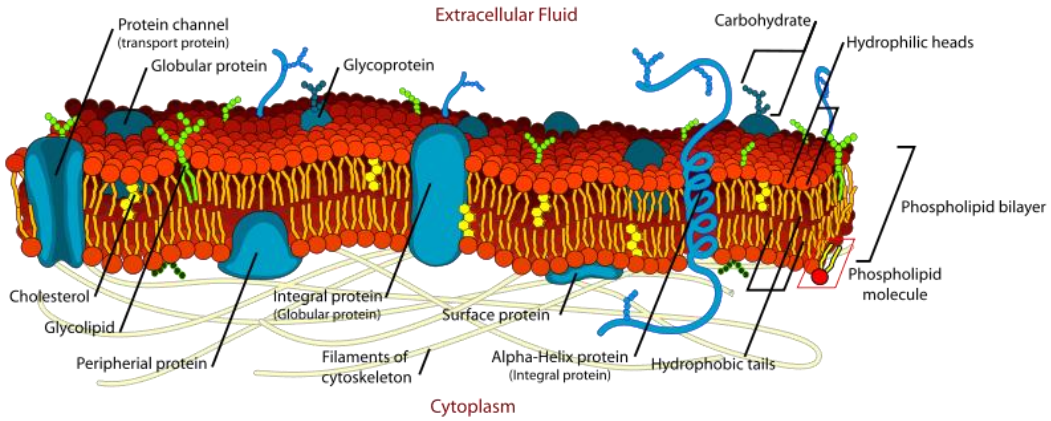

Figure 2.1 Lipidic Bilayer including integral and peripheral proteins forming the Cell Membrane

Note that his Image has been downloaded from the University of New South Wales-Sidney. Available at http://cellbiology.med.unsw.edu.au/units/science/lecture0803.htm

Each monolayer has its hydrophobic surface oriented inward and its hydrophilic surface outward towards either the intra- or extracellular fluids. The intrinsic electrical conductance of this structure is very poor, of the order or 10^{-6}S/m and it is considered as a dielectric material. An important property of a dielectric is its ability to support an electrostatic field and therefore storage energy. The total structure formed by the intracellular fluid, plasma membrane and extracellular fluid forms a conductor-dielectric-conductor alike structure behaving as a capacitor, with an approximate capacitance of 1 μF/cm^2.

2.1.3. The Dispersion Windows

The passive electric properties of biological tissue present certain dependency on the frequency. Therefore the frequency spectrum of the electrical conductivity and permittivity is not constant presenting four transition regions, which are known as dispersion windows, can be observed. The classification of the dispersion windows is based on the electrical examination of biomaterials as a function of frequency that is known as dielectric spectroscopy. H.P. Schwan divided the relaxation mechanisms initially in 3 groups, [11] and later in 4 groups, providing the four identified dispersion windows. Known as α, β, δ and γ-dispersions.; see Figure 2.2.

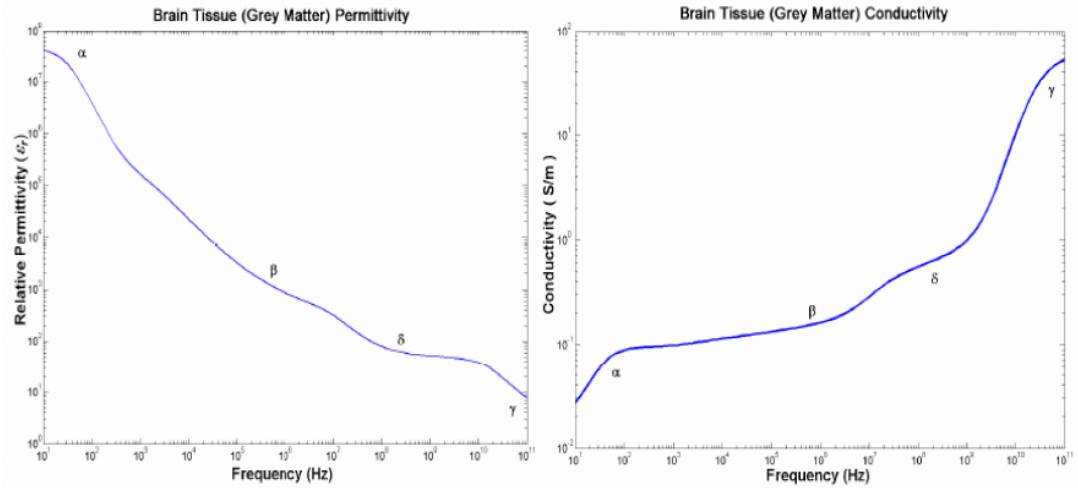

Figure 2.2 Frequency dependence of the conductivity and permittivity of brain grey matter. Plots from [3]

2.2. Measurements of Electrical Bioimpedance

2.2.1. The Cell Membrane

The electrical properties of the tissular constituents confer a frequency dependency to the electrical bioimpedance and therefore any proper equivalent electrical models should represent such dependency. H. Fricke in 1924 [5] proposed a simple electrical equivalent model made by resistors and capacitors, see Figure 2.3.

In Figure 2.3 a) and b) the capacitor *Cm* represents the membrane, *Rm* represents the resistance of the ionic channels (high value due to their low conductivity) and *Re* and *Ri* represent the extra cellular and intracellular fluids respectively. Fricke's model is depicted in Figure 2.3 c)

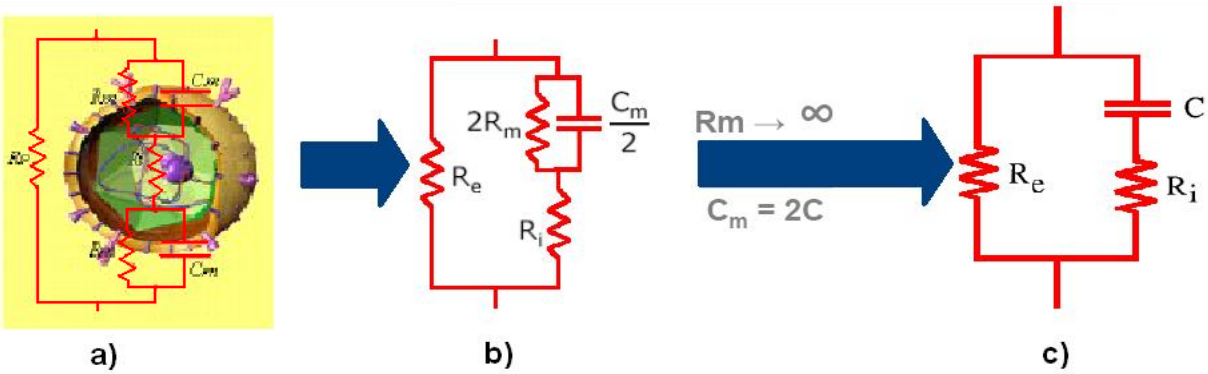

Figure 2.3 Equivalent circuit of a cell where *Re* is the extracellular fluid Resistance, *Ri* the intracellular fluid Resistance, *Rm* the trans-membrane ionic channel Resistance and *Cm* represents the cell membrane Capacitance.

and notice that the resistance of the membrane has been neglected due to its extremely large value.

The impedance spectrum of a cell according to Fricke's model is given by the following equation:

$$Z(\omega) = \frac{R_e(1+jR_iC\omega)}{1+jC\omega(R_e+R_i)} \qquad (2.1)$$

According to this simplified model, the electrical behavior at high and low frequencies can be explained as follows:

- At low frequency, the membrane impedance is very high and only a small portion of the current flows through the cells and most of the current flows through the extracellular fluid as shown in the left side of Figure 2.4. Therefore the impedance is represented by only *Re*.

- At high frequency, the capacitive effect of the plasma membrane decreases and the current flows through the intra and the extracellular fluid as shown in the right side of Figure 2.4. Thus, the value of the equivalent impedance becomes the parallel between resistances of the intra and the extracellular fluid, *Ri*||*Re*.

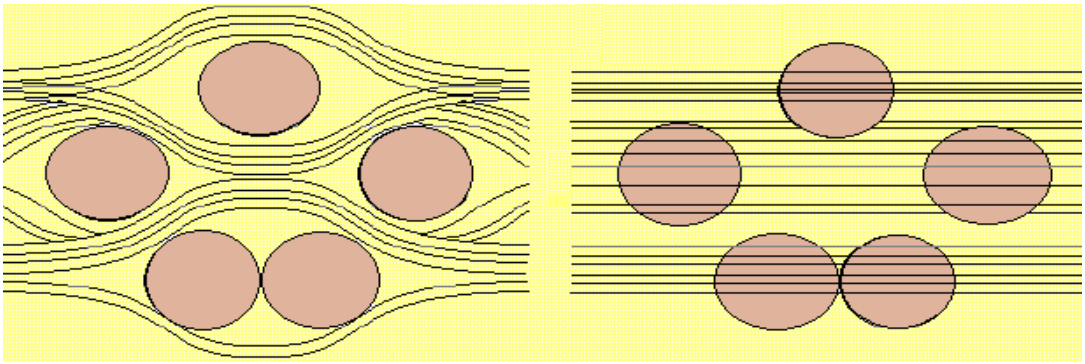

Figure 2.4 Current paths in a suspension of cells at low and high frequencies.

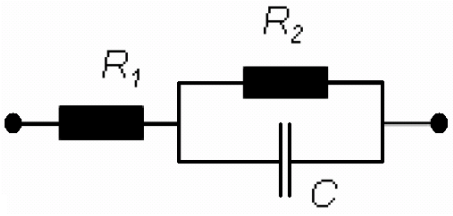

Figure 2.5 Equivalent model used for skin tissues

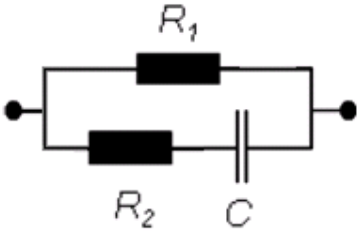

Figure 2.6 Equivalent model typically used for suspension of cells

Biological tissue contains various different types of cells in several different arrangements and following the same approach applied by Fricke on the frequency range of the Beta-Dispersion, explanatory and descriptive models can be obtained with circuit bridges. Figure 2.5 presents a series circuit bridge and Figure 2.6 presents a parallel circuit bridge.

2.2.2. Cole Model and Cole Plot

Electrical Bioimpedance is a measurement of the ability of a material to create an opposition to the flow of electric current through the tissues and the impedance is denoted by Z. The impedance can be represented mathematically as a complex magnitude in cartesian coordinates, made up of two components, Resistance (R) and Reactance (X) (2.2), or in polar coordinates using magnitude (|Z|) and phase (θ) (2.3).

$$Z = R + jX \quad \textbf{(2.2)}$$

$$Z = |Z|e^{j\theta} \quad \textbf{(2.3)}$$

The electrical impedance of linear systems is ruled by Ohm's law, which relates voltage in volts and current in Amperes through an impedance in Ohms, as denoted in (2.4).

$$Z = \frac{V}{I} \quad \textbf{(2.4)}$$

Based in Ohm's law, a deflection method to measure electrical bioimpedance consist on applying electrical current or voltage on the tissue and measure the response of the tissue to the electrical stimulus. Like the input value over the impedance load is know and the complementary value is measured, it is possible to obtain the value of the impedance load with Ohm's law. Most often the electrical stimulus is applied into the tissue through electrodes and the electrical response is also measured with electrodes. Therefore in order to do EBI measurements there are several electrode configurations available and some of them they will be explained in the following section.

2.2.3. Electrode configuration

There are several electrode configurations, but in this section only two will be explained: The 2-Electrode and 4-Electrode configuration, which are the configuration relevant to this work.

2-Electrode configuration

With this configuration, depicted in Figure 2.7, both electrodes are used to inject the electrical stimulus and to measure the response produced by the tissue. Therefore, in this configuration the electrode-electrolyte interface impedances are in series with the sample impedance providing a total measured voltage V_{MEAS} containing the sum of the voltages caused by the three impedances, see (2.5).

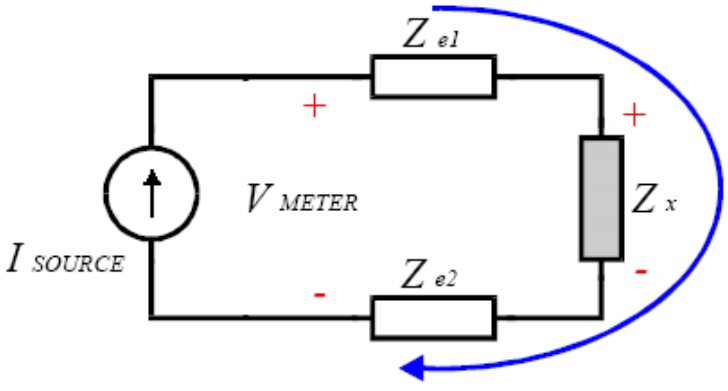

Fig 2.7 Two electrodes configuration.

$$Z_{MEAS} = \frac{V_{MEAS}}{I_{SOURCE}} = Z_x + Z_{e1} + Z_{e2} \quad \textbf{(2.5)}$$

Therefore the impedance obtained by applying Ohm's law is the combination of the tissue impedance together with the electrode impedance. Unfortunately, these impedances can be difficult or almost impossible to separate and alternative measurement method must be used: The 4-Electrode configuration.

4-Electrode configuration

In this method the electrical stimulus is applied with a pair of electrodes and the resulting response is measured with a different pair of electrodes, see Figure 2.8. Focusing on a current driven system, the voltage on the current injecting electrodes is not contained in the voltage response sensed by the system, therefore the influence of the electrodes impedance can be reduced (2.6).

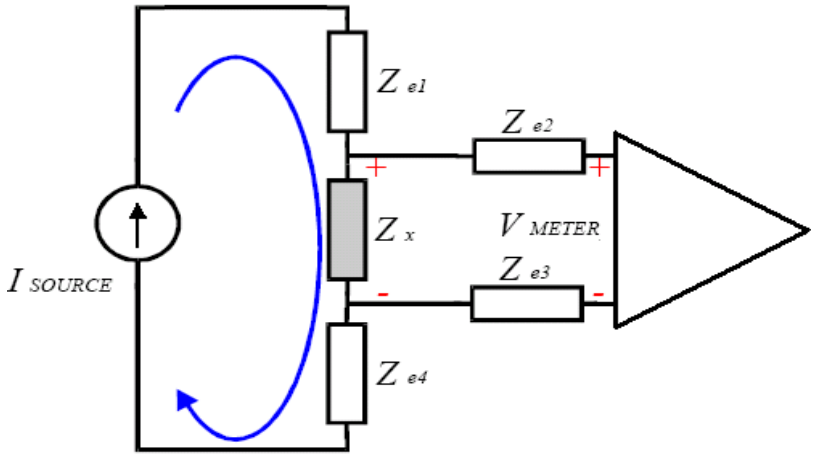

Figure 2.8 Four electrodes configuration for a current driven system

$$Z_{MEAS} = \frac{V_{MEAS}}{I_{SOURCE}} = Z_X \quad \textbf{(2.6)}$$

2.3. Applications of Bioimpedance

To analyze EBI data for each of the applications that have been studied in this work, several approaches are available. In this section several methods used to obtain Body Composition parameters as well as the applications of Respiration Rate and Lungs Composition will be introduced.

2.3.1. Body Composition

The measurement of body fluid volumes, see Figure 2.7, Extra Cellular Water (ECW), Intra Cellular Water (ICW) and their sum, total body water (TBW) is important in many pathologies. TBW is strongly related to Fat-Free-Mass (FFM) which contains, in healthy individuals, an average of 73.2% of water [12].

Similarly, Body Cell Mass (BCM), which is an important nutritional parameter, is also closely connected to ICW. Independent measurements of FFM and TBW permit to detect dehydration, which is frequent in elderly persons or athletes after heavy training. Conversely, an overhydratation may indicate the presence of edema in cardiac patients of lymphoedema after a mastectomy. The measurement of TBW is also useful for evaluation of diuretic therapy. Renal patients treated by hemodialysis accumulate fluid between treatments. It is important to evaluate their amount of excess fluid, in order to determine how much fluid they should lose by ultra filtration and also how this fluid loss is distributed between ECW and ICW. Measurements of BCM are also important for assessing the morbidity of patients infected by HIV [13].

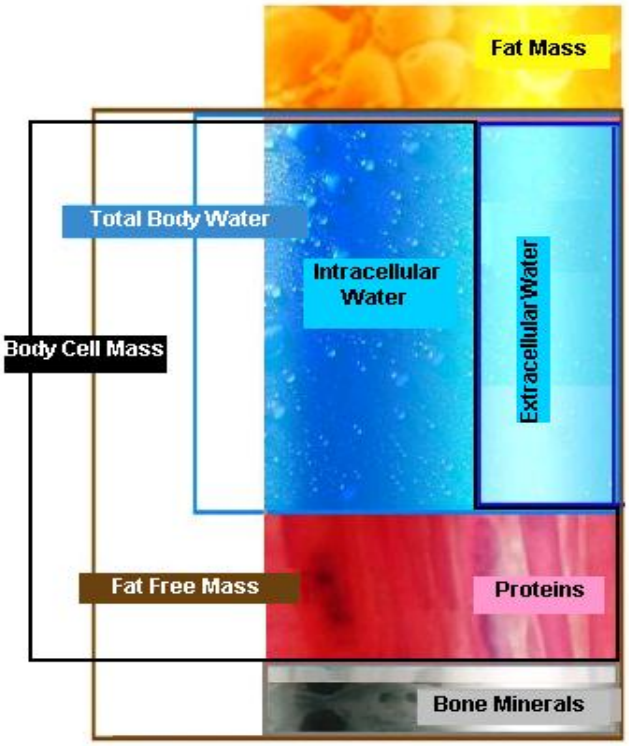

Figure 2.7 Schematic of fat-free mass, total body water, intracellular water, extracellular water and body cell mass.

For Body Composition analysis there are several EBI methods available and two of them; BIA Analysis and BIVA will be introduced in the following sections.

2.3.1.1. BIA Analysis

Bioimpedance analysis (BIA) is a very well widespread method for assessment of Body Composition. It consists in the measurement of the impedance or opposition to the flow of an electric current through the body fluids contained mainly in the lean and fat tissue. Impedance is low in lean tissue, where intracellular fluid and electrolytes are primarily contained, but high in fat tissue. Impedance is thus proportional to TBW value. Due to the impedance in lean tissue, where intracellular fluid and electrolytes are primarily contained, is lower than in fat tissue and because of the measured body resistance differs depending on the amount of body fluids, it is

possible to estimate the body composition. The basic model of this method is depicted in Figure 2.8 and it is based on the assumption that the body is a cylindrical-shape ionic conductor. In such volume conductor, the impedance between faces of a cylinder of finite length L and a cross sectional area A, when a uniform current density is applied parallel to its axis, is given by (2.7)

$$Z = \rho^* \frac{L}{A} \tag{2.7}$$

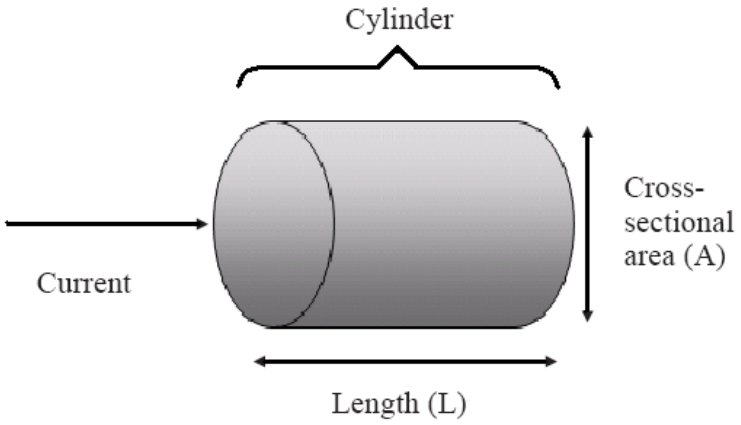

Figure 2.8 Principles of BIA from physical characteristics to body composition. Cylinder model for the relationship between impedance and geometry.

The measured impedance is a function of both the tissue complex resistivity ρ and also the shape of the conductor. Although the body is not a uniform cylinder and its conductivity/resistivity is not constant, a relationship between the volume of body water (V) and the ratio length (L) to impedance can be established as in equations (2.8) and (2.9) [14].

$$Z = \rho^* \frac{L^2}{V} \tag{2.8}$$

$$V = \rho^* \frac{L^2}{Z} \tag{2.9}$$

It is easier to measure height than the conductive length, which is usually from wrist to ankle. Therefore, the empirical relationship denoted as in the equation 2.10.

$$TBW = K^* \frac{Heigt^2}{Z} \tag{2.10}$$

Due to the inherent inhomogeneity of the human body, and that (2.9) holds true for a homogeneous cylinder, the coefficient K in (2.10) describes an equivalent cylinder, which must be adjusted to match the real geometry. The value of the coefficient depends on various factors. More information can be obtained reading [15].

With the aim to obtain the body composition parameters the follow BIA methods are currently used:

- Single Frequency-BIA
- Multi Frequency-BIA
- Spectroscopy-BIA
- Segmental-BIA

2.3.1.2. Single Frequency BIA

Single Frequency Bioimpedance Analysis (SF-BIA) methods rely only on the whole-body impedance (Z50) or the resistance (R50) measured at 50 KHz between the wrist and the ankle, as shown in Figure 2.9. Impedance data are subsequently entered into predictive equations derived through statistical regression in order to determine TBW, from which FFM is calculated according to the assumption that FFM is hydrated at 73.2% [16].

Several studies showed that a frequency of 50 kHz is too low for full penetration of current through the cell [17]. Theoretically, these devices are unable to discriminate between ECW and ICW. Therefore, the use of these new devices is not recommended in cases of abnormal fluid distribution. *i.e. pathological cases.*

2.3.1.3. Multi frequency BIA

As with SF-BIA, Multi Frequency Bioimpedance Analysis MF-BIA uses empirical linear regression models but includes measurement of impedance at multiple frequencies. MF-BIA uses impedance data measured at least 2 frequencies: 1 at a very low frequency, usually 5 kHz, and 1 at a high frequency, typically 50, 100, 200, or 500 kHz, to evaluate FFM, TBW, ICW and ECW [18]. At the lowest frequency, measurements of impedance can be used to determine ECW. At

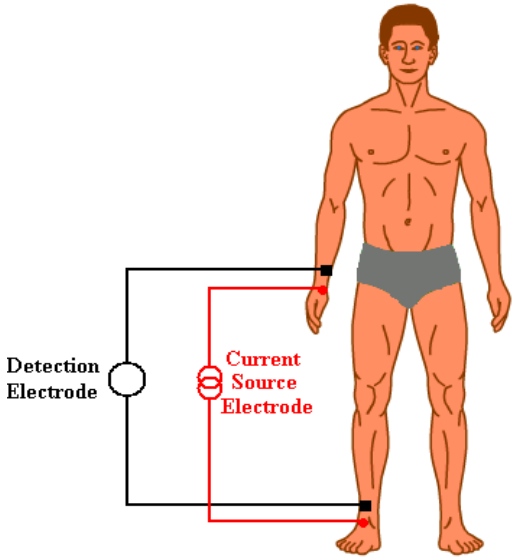

Figure 2.9 Standard placements of electrodes for wrist to ankle 4E-measurements for SF-BIA and MF-BIA applications.

higher frequencies, the current can pass through the cell membrane, and thus, the impedance measurements can be used to determine TBW. The impedance data are applied to regression-derived equations in order to predict TBW, ECW, and ICW. According to [19] MFBIA is more accurate and less biased than SF-BIA for the prediction of ECW, whereas SF-BIA, compared to MF-BIA, is more accurate and less biased for TBW in critically ill subjects. [20].

2.3.1.4. Spectroscopy BIA

Spectroscopy Bioimpedance Analysis operates on impedance data measured over a wide spectrum of frequencies, usually from 5 to 1000 kHz. To analyze the BIS-derived impedance data, the most practical approach for clinical applications is to perform biophysical modeling on the impedance data; the modeling procedure involves fitting the spectral data to the Cole model using nonlinear curve fitting [21] [13]. This procedure generates the Cole model parameters, as well as R_0, R_∞, τ and exponent α. Cole model terms are then applied to equations derived from the Hanai mixture theory [22], which is essentially based on the notion that the body is a conducting medium of water, electrolytes, and lean tissue, in addition to non-conducting material within it. ECW and ICW are thus calculated individually; TBW is calculated as the sum of ECW and ICW.

Bioimpedance Spectroscopy Analysis provides a more direct, individualized measurement of ECW and ICW than other bioimpedance approaches. This is due, in large part, to the fact that it measures impedance over a broad spectrum of frequencies, rather than being limited to only 1 or 2 frequencies, like in the case of SF-BIA and MF-BIA, respectively. Of particular importance, BIS differs from SF-BIA and MF-BIA in that it does not rely on statistically derived regression equations to predict body water volumes. Furthermore, it relies far less on assumptions that may be violated in disease states. For example, 2 assumptions underlying the SF-BIA method that may not hold true in many clinical populations are that FFM is 73% hydrated and that ICW and ECW are normally distributed.

2.3.1.5. Segmental BIA

Segmental Bioimpedance Analysis, the body is considered to comprise five interconnecting conducting cylinders, two legs, two arms, and the trunk, as shown in Figure 2.10.

Although the trunk of the body represents as much as 50% of whole body mass, it only contributes around 10% to whole body impedance. This implies three aspects for body composition analysis when using the whole body-one cylinder- BIA approach:

- Changes of the impedance are closely related to changes of the FFM of the limbs.
- Changes of the FFM of the trunk are probably not adequately described by whole body impedance measurements
- Even large changes in the fluid volume within the abdominal cavity have only minor influence on the measurement of FFM or BCM.

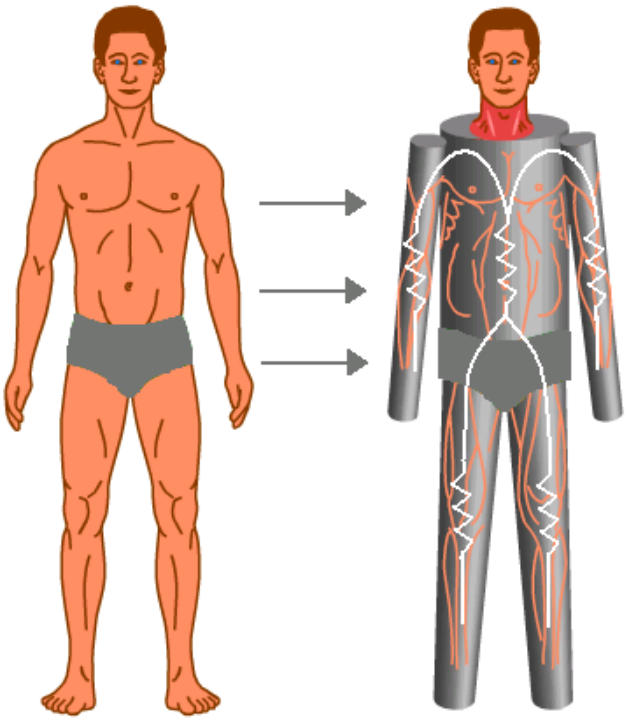

Figure 2.10 Five-Cylinder model of the body and the impedance for each segment: right arm, right leg, left arm, left leg, and trunk.

2.3.1.6. BIVA Analysis

In Piccoli et al (1994) the RXc-graph method was proposed. Resistance, R and reactance, Xc are obtained with right-side configuration in SFBIA at 50 kHz after standardization by height H. In contrast to other bioimpedance methods this approach does not yield any absolute estimate of ECW, ICW or TBW, makes no assumptions about body geometry, hydration state, or the electrical model of cell membranes and is unaffected by regression adjustments.

In BIVA, Z can be considered as a bivariate random vector: resistance R and reactance Xc. These two variables, standardized for height, are plotted as point vectors in the R–Xc plane. An individual vector can then be compared with the reference 50%, 75%, and 95% tolerance ellipses calculated in the healthy population of the same gender and race. That is called R–Xc graph method; see Figure 2.10. The ellipse varies with age and body size. For more information see [15]

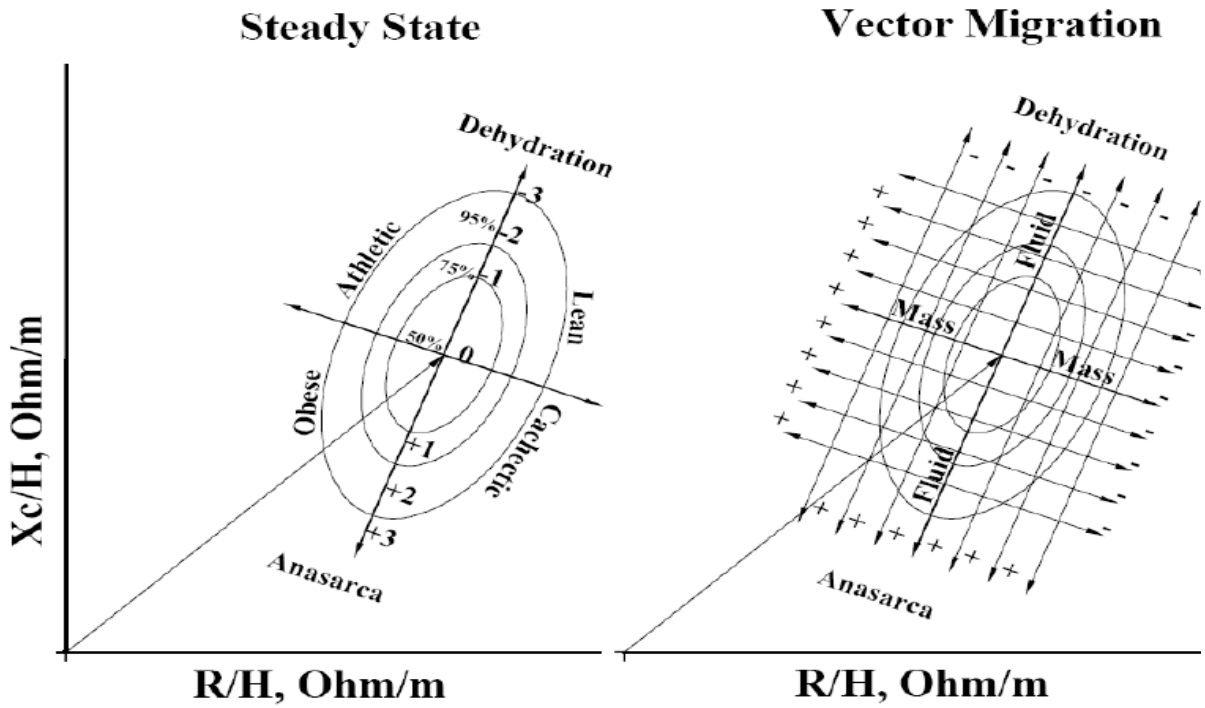

Figure 2.11 BIVA Pattern (RXc-graph) [2].

2.3.2. Respiration Rate (Impedance Pneumography)

Impedance pneumography is a non-invasive technique for monitoring the respiration rate and involves measuring changes in the electrical impedance of the thoracic cavity. The resistivity of lung tissue increases due to the thinning of the alveolar walls as well as by the deformation of the epithelial cells and blood vessels through the expansion of the alveoli [23]. These changes in resistivity combined with diaphragm movements and changes in the chest circumference affect the overall impedance of the thoracic cavity during breathing [24]. Even though there exists a good correlation between the volume of inspired air and impedance of the thoracic cavity as pointed in [25] the volume of air in the lungs is not the responsible for the change in resistance.

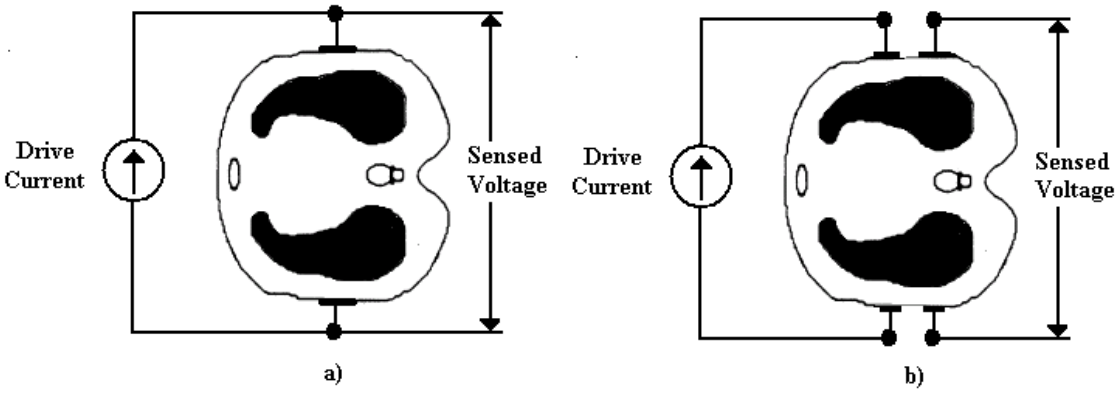

Figure 2.12 Electrode configurations for pneumography impedance measurements. In a) and in b) are respectively showed the bi-polar and the tetra-polar configuration.

These impedance changes are measured by injecting a low-amplitude, single high-frequency, constant current using a pair of ‘drive’ electrodes and recording the resultant voltage changes either from the same pair of electrodes as in a 2-Electrode (bi-polar) configuration in the Figure 2.12.a or from a different pair of ‘receive’ electrodes placed at an appropriate location as in a 4-Electrode (tetra-polar) configuration in the Figure 2.12.b [26].

Impedance pneumography is well tolerated by patients because it does not involve placing any device within the airway that may cause discomfort to the patient. Therefore, it is the most widely used technique for the purpose of long-term monitoring and home monitoring.

2.3.3. Lungs Composition (Impedance Plethysmography)

The impedance plethysmography is a non-invasive technique used to detect the changes of the thoracic impedance. It is known that changes of the thoracic impedance correlate with changes of the clinical syndromes of a lung edema due to the accumulation of fluid in the lungs [27] [28], see Figure 2.13. Furthermore, the thoracic impedance decreases considerably before the first clinical syndromes appear. So lung edema can be well detected using impedance plethysmography during their appearance and disappearance.

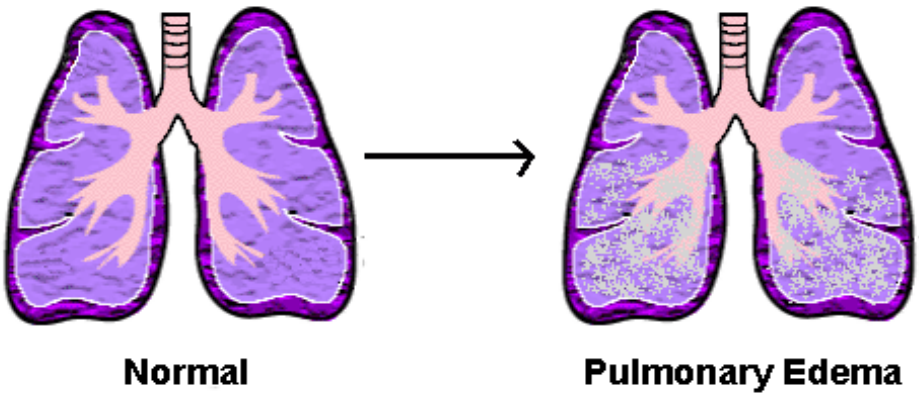

Figure 2.13 The figure illustrates in the left hand normal lungs and in the right hand lungs with Pulmonary Edema. The light blue color on the right side drawing represents water.

The electrode placement for measurements of lung edema is under investigation, but there are two methods commonly used. The first method is the tetra polar configuration, as the Figure 2.14.a shows and the other method uses 6 electrodes in the specific placement as shows the Figure 2.14.b.

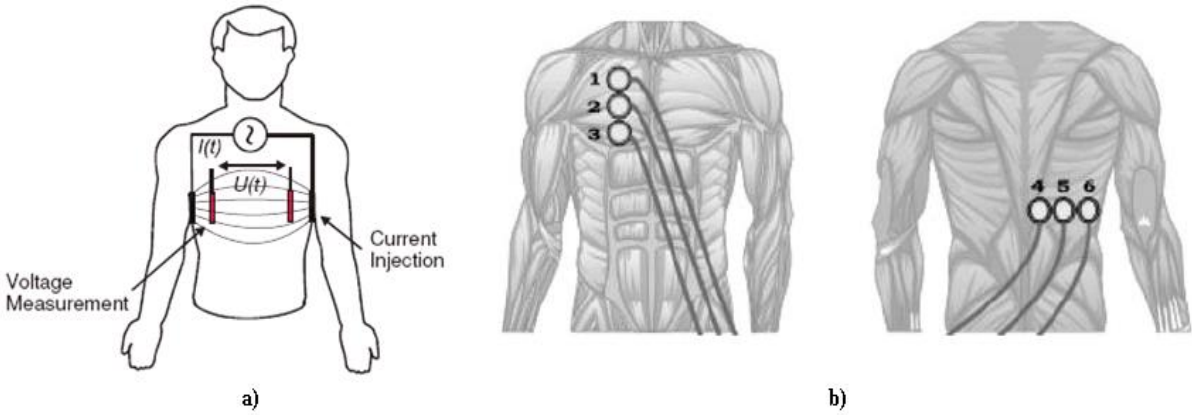

Figure 2.14 Thoracic bioimpedance measured in the tetra polar configuration in a) and the with six electrodes configuration in b).

3.1. Instrumentation

In this section the instrumentation and materials needed to realize this thesis work will be introduced. In order to perform the spectroscopy EBI measurements obtained in this work, two impedance meters have been used: The SFB7 spectrometer manufactured by Impedimed and the custom made spectrometer based on the evaluation board for the Impedance Converter Network Analyzer AD5933 plus a 4-Electrode enabling- Analog Frond End [29].

3.1.1. SFB7 Body Composition Analyzer

The Imp SFB7, shown in Figure 3.7, accurately measures current, voltage and phase angle to calculate the complex Electrical Bioimpedance, both resistance and reactance in a wide frequency range. The impedance meter utilizes Cole modeling with Hanai mixture theory for body composition assessment for determining the following Body Composition parameters from impedance data:

- Total body water (TBW)
- Extracellular fluid (ECF)
- Intracellular fluid (ICF)

Figure 3.1 The Imp SFB7 is a 4-Electrode EBI spectrometer and back connection for the 4E-Electrodes

The device has 3 modes of operation but only one mode has been used for the realization of this work: The MFBIA mode. This mode is mainly use for Bioimpedance Spectroscopy,

measuring complex bioimpedance over a frequency range of 3.084 - 1024 kHz by sweeping through 256 frequency measurement points. The screen of the Imp SFB7 displays the measured data in the form of a Cole plot, a resistance vs. frequency and a reactance vs. frequency plots, see Figure 3.2. In addition the characteristic frequency and the Cole parameters are estimated for each measurement as well as the aforementioned Body Composition Analysis parameters.

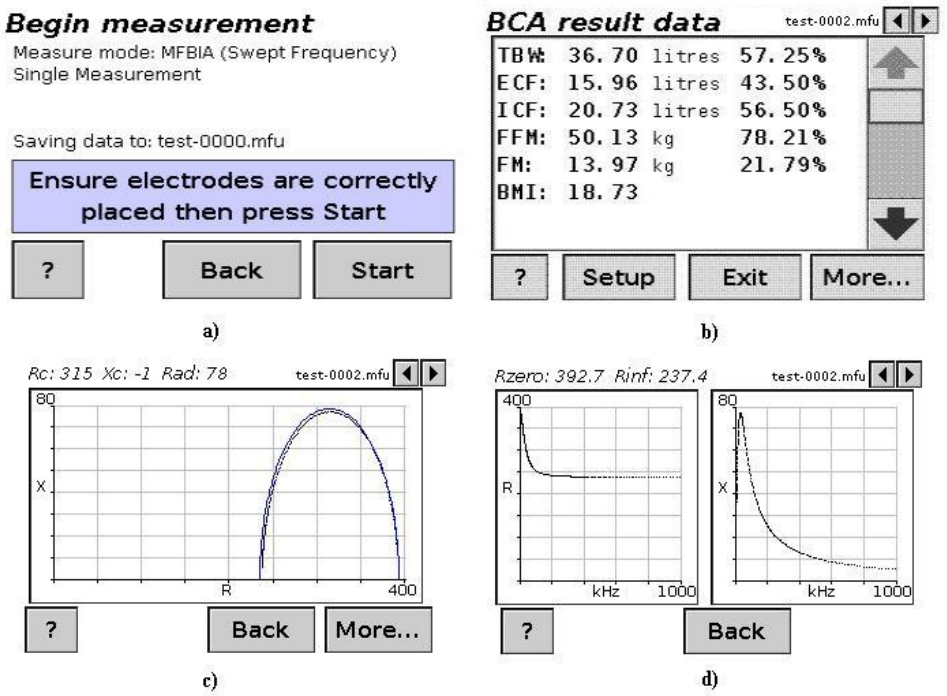

Figure 3.2 Screenshots of a MFBIA measurement with the Imp SFB7 device. The figure shows in a) the Measure Mode, in b) the BCA results data, in c) Impedance Cole plot and in d) resistance vs. frequency and reactance vs. frequency.

In any of the operation modes, several EBI measurements can be performed well continuously or at selected intervals of time, storing over 1000 records on the internal memory of the device.

For more information about the operation modes the reader is referred to the User's manual of the Imp SFB7.

3.1.2. The BioImp Software

The Impedimed BioImp software application analyses and displays multi-frequency data measured with the Impedimed Imp SFB7 device. Figure 3.3 contains a screen-shot of the software. It can also be configured to read and analyze ASCII text files of multi-frequency impedance data from other sources.

The application presents the impedance data to the user as charts showing resistance and reactance plotted against frequency and also a Cole plot. Note that the software indicates that the

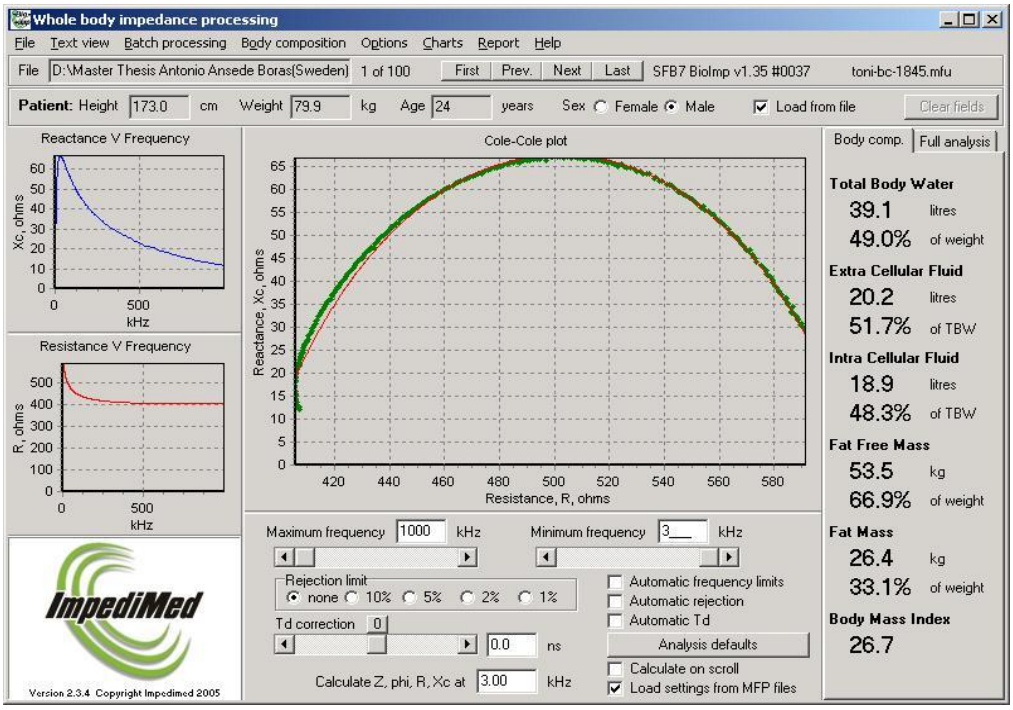

Figure 3.3 The Impedimed BioImp applications displaying whole body bioimpedance data from the Impedimed Imp SFB7 device.

impedance plot is a Cole-Cole Plot but that is wrong, since the plot is in the impedance plot and the Cole-Cole plot do not represents impedance data. The data analysis fits a Cole model curve to the measured data, and derives body composition estimates from the Cole model. There are adjustable input parameters for the fitting algorithm. The source data and analysis results can be viewed in text form and in graphical form.

3.1.3. Evaluation Board for the Impedance Converter Network Analyzer AD5933

The main component of the evaluation board in Figure 3.6 is the IC manufactured by Analog Devices: the AD5933, see functional block on Figure 3.4. The AD5933 is a 12-bit precision impedance converter which combines an onboard frequency generator with a 1 MSPS Analog-to-Digital Converter (ADC) and a Digital Signal Processor (DSP) engine which performs the impedance estimation. The AD5933 operates from a 2.7 V to 5.5 V power supply. The evaluation Board has the option to power up the entire circuitry from the USB port of the computer and it has an accurately trimmed 16 MHz crystal to act as a system clock to the AD5933 as well, if it is required.

The AD5933 includes a serial I_2C port as communication interface that allows the adjusting of several operational parameters as well as the transmission with an external Host of the impedance data results. In order to make the interface between the I2C signals from the AD5933 with USB the board has a USB microcontroller that produces de I2C-USB conversion, see Figure 3.5.

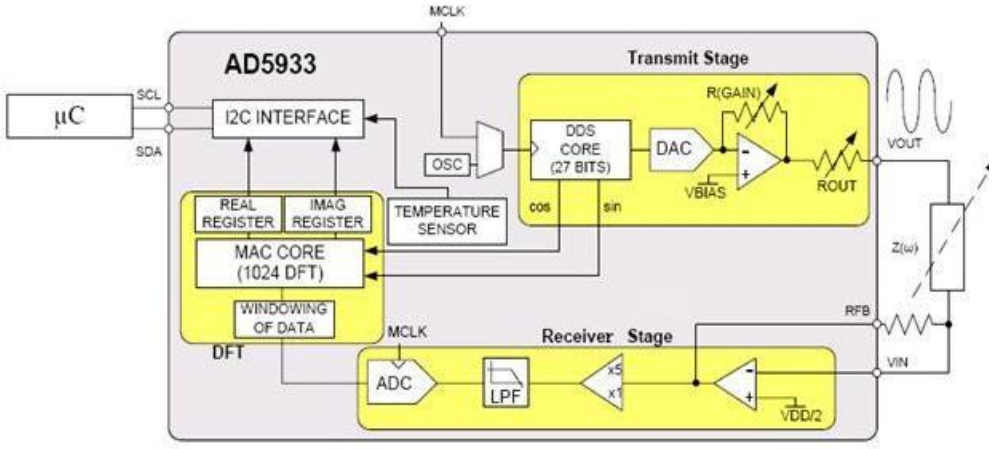

Figure 3.4 The functional block diagram of the IC AD5933

The AD5933 circuit allows the user to perform a frequency sweep with a user defined start frequency, frequency resolution, and number of points in the measurement sweep. In addition, the device allows the user to program the peak-to-peak value of the sinusoidal output signal as an excitation to the external unknown impedance under test connected between the VOUT and VIN terminals. The excitation signal for the transmission stage is provided on-chip using Direct Digital Synthesizer (DDS) techniques, which permit subhertz resolution. The AD5933 offers a frequency resolution programmable by the user down to 0.1 Hz. As a response to the voltage excitation, a corresponding electrical current flows through the load. This current will be sensed at the receiver stage and the ratio between its value and the value of the excitation voltage will be used to estimate the impedance value. The clock for the DDS is generated from either an external reference clock which is provided by the user at MCLK or by the internal oscillator.

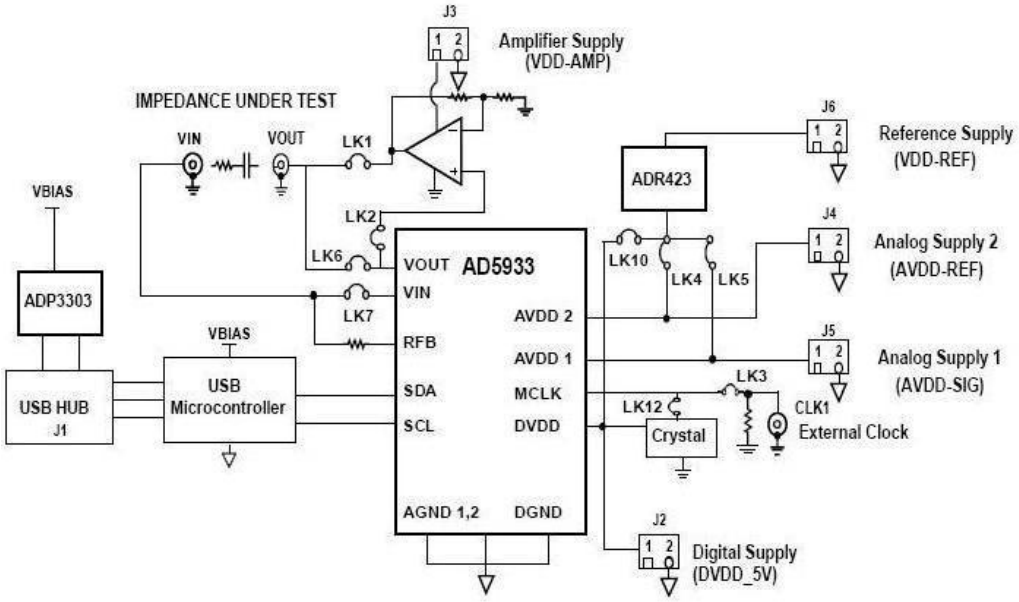

Figure 3.5 The block diagram of diagram block of the AD5933 evaluation board

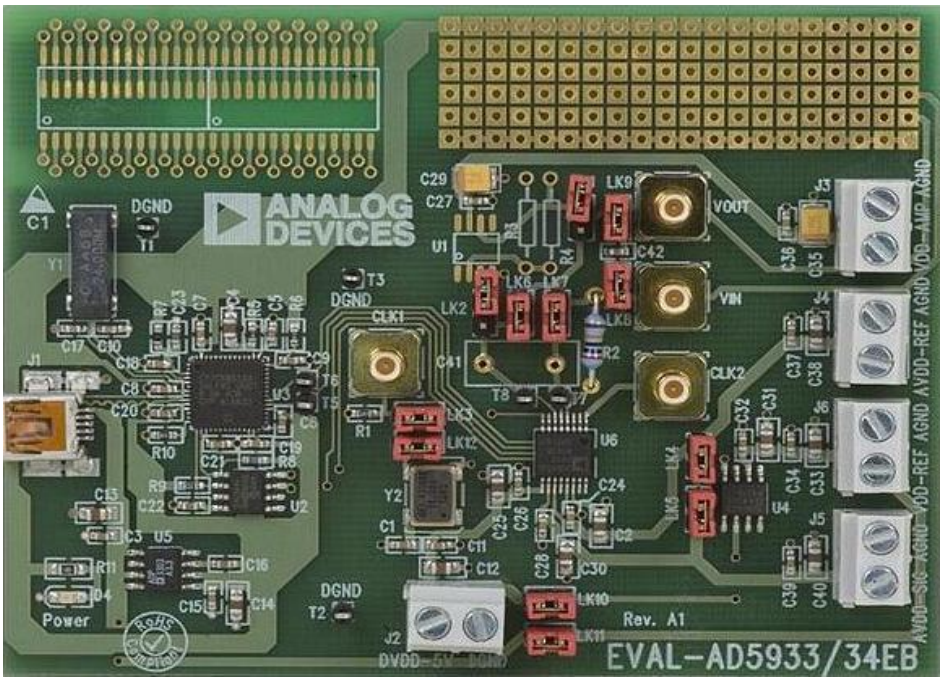

Figure 3.6 The evaluation board manufactured by Analog Devices.

For detailed information about the evaluation board for AD5933, please read the datasheets of the AD5933 and the AD5933 evaluation board.

3.1.4. Four Electrodes Analog Front End

Since the AD5933 is a 2-Electrode measurements system and its electrical stimulation does not comply with the safety regulations, the evaluation board is connected to an Analog Front-End (AFE) circuit [29]. The functionality of this AFE is twofold:

- To ensure that the safety conditions regarding current injection for performing EBI measurements in human patients are fulfilled. Basically this means that the electrical signals are below any safety threshold and no DC current is introduced in the body.

- To adapt the AD5933 operation from a 2-Electrode measurement system to a 4-Electrode measurement system. This way the polarization impedance of the electrodes is removed from the EBI measurement and the system can be used in applications of spectral characterization. The AFE is connected to the evaluation board through two cables and to the patient through 4 electrodes.

In short, we could consider the AFE, see Figure 3.7, as a combination of two Voltage-to-Current converters (V2CC), one in the direction from the AD5933 and another from the TUS to the AD5933.

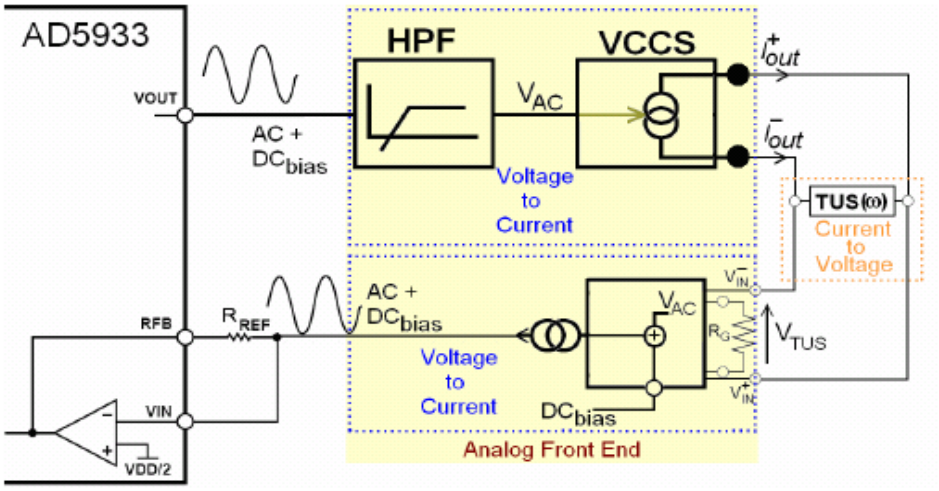

Figure 3.7 Functional block diagram of the Analog Front-End.

Since the AD5933 applies voltage and expects a current at its input RFB, the AFE interfacing with the AD5933 has a voltage input and a current output. Source output expressly generates a current resulting from the ratio from Vout and the impedance of the Tissue Under Study (TUS), which is the exactly the current expected by the AD5933 at the input RFB as indicated in Figure 3.7. At the TUS side, the AFE has a current source as output, exciting the TUS with 350 µA-rms, while the input is a differential voltage measurement channel.

In essence the AFE operation can be describe as follows: after the removal of the DC bias component from the voltage output of the AD5933 with a low pass filter at the input of the first V2CC, the AC voltage from Vout drives the Voltage Controlled Current Source (VCCS) injecting an AC current Iout in the TUS directly proportional to Vout.

The second V2CC senses at its differential input the voltage drop caused at the TUS by the AC current generated by the first V2CC flowing through the TUS. Finally an AC current proportional to the voltage drop in the TUS is generated at the output of the second V2CC with an added DC component equivalent to the DCbias removed originally from the Vout. The total gain introduced by the cascade combination of both V2CC in the AFE is selectable by the choosing of several resistors.

3.2. Method

In order to evaluate the performance of the Impedance Spectrometer On-chip AD5933 +4-Electrode Analog Frond End (4E-AFE), Impedance spectroscopy measurements for several EBI applications have been taken. Experimental measurements on electrical equivalent models have been taken with the AD5933+4E-AFE system and the EBI spectrometer Impedimed SFB7. The obtained impedance spectral data have been used to estimate the values of the equivalent circuit under measurement and the estimated values have been mutually compared in terms of estimation accuracy.

The measurements have been taken on 2R1C equivalent models [30], each of them representing an specific EBI application. The electrical equivalence has been established both in terms of frequency as well as Ohmic load dynamic range. The values of the passive electrical components models were obtained experimentally from experimental EBI measurements. Since the value of the working load depends on the EBI applications, the functioning of the AD5933+4E-AFE was adjusted specifically to the impedance values range of each model. Figure 3.8 shows the work flow that has been applied in this work.

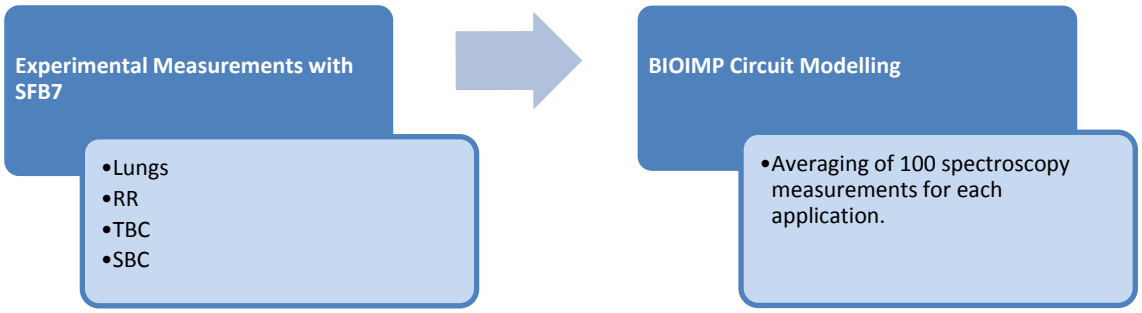

Figure 3.9 Modeling process overview

3.2.1. Application Equivalent Modeling

The equivalent circuit topology chosen to model the EBI applications has been the 2R1C [30]. To obtain the values of the passive components for each specific equivalent model, the following steps have taken:

1. Experimental Measurements. In this step EBI measurements have been taken in a healthy subject for the following EBI applications:

   - Total Body Water contents
   - Lungs Composition
   - Respiration Rate
   - Segmental measurements for Body Composition:
     Arm-Arm, Leg-Leg, Trunk-Trunk.

   The specific morphological data of the subject is shown in Table 3.1.

TABLE 3.1

Sex	Age (years)	Length(cm)	Weight(Kg)
Male	24	173	79

   The 4-Electrode EBI measurements were taken with the SFB7 spectrometer within the frequency range 3 kHz to 1 MHz.

2. BioImp 2R1C-paralell bridge Circuit Modeling. The obtained spectral impedance data from each of the EBI application specific measurements were processed with the BioImp software to obtain the values for the passive components of the equivalent circuit model.

   The obtained values and parameters obtained from each EBI applications are the following:

   - 2R1C model components:
     - Intracellular Resistance (*Ri*)
     - Extracellular Resistance (*Re*)
     - Membrane Capacitor (*Cm*)
   - Resistance at 0 Hz (R_0)
   - Resistance at ∞ Hz(R_∞)
   - Characteristic Frequency (*Fc*)

   The final value for each of the parameters was obtained from the averaging of 100 spectroscopy measurements using the batch processing tool available at BioImp.

3.2.2 EBI Application Equivalent Load

Once typical values for the components of the 2R1C have been calculated by averaging the experimentally performed EBI measurements, a typical dynamic range for the resistance was obtained. The maximum value of the model is set by *Re* and the minimum is set by the parallel connection of *Re//Ri*.

Since the circuit parameters have been obtained from a single subject and both *Re* and *Ri* have an strong dependency on the size and the form of the tissue under study *i.e.* the whole body. The values of the resistors of the 2R1C bridge have been adjusted considering for the variance in morphological parameters of the population *i.e.* size, complexion, high etc. The applied process is explained as follows in the next diagram, see Figure 3.10.

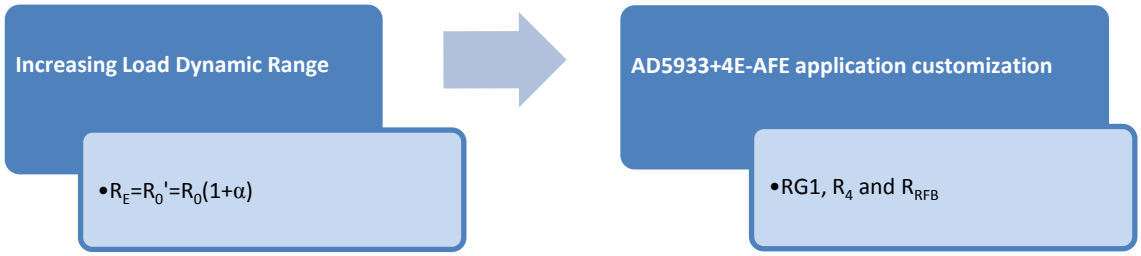

Figure 3.10 EBI Application Equivalent Load and Customization Process Overview

1. Increasing the Load Dynamic Range. The range of values of the load was increased not directly over the 2R1C model but on the Cole parameters. Since the EBI spectrometer measures bioimpedance down to 0 Ohms, the upper limit of the range was adjusted modifying the value of R_0. The new R_0' value was obtained by

using a multiplicative factor (1+α) for R_0, where α is a constant set to 0.5. *i.e. the value of R_0 was increased 50%,* see Equation 3.1.

$$R_0' = R_0(1 + \alpha) \quad \textbf{(3.1)}$$

Due to this modification the values of the equivalent 2R1C model for the resistances *Ri* and *Re* and *Cm* were recalculated aiming to keep the original frequency dependency. The value recalculation was done as follows. The 2R1C circuit was simplified for D.C:

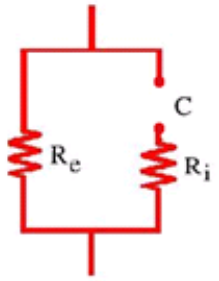

Figure 3.11 2R1C parallel Bridge for f=0

According to the previous figure *Re*' is equal to R_0', that is the maximum value of the resistance that the EBI spectrometer will measure for a given EBI application and therefore the AD5933, will be adjusted for a RTUS max equal to the newly obtained *Re*' to make the best use of the ADC. See Equation 3.2.

$$R_{TUS\_max} = R_e' \quad \textbf{(3.2)}$$

In order to keep the value of the characteristic frequency of the 2R1C similar to the typical value of each corresponding EBI application, the value of *Ri* was recalculated keeping the obtained value of *Re*' and the original value of *Cm* as follows in Equation 3.3.

$$Ri' = \frac{1-2*\pi*Cm*Fc*Re'}{2*\pi*Fc*Cm} \quad \textbf{(3.3)}$$

The calculated values were used to build the equivalent electrical model 2R-1C for each application. Each model was implemented with a resistor as *Re*, a capacitor as Cm and a potentiometer for *Ri* with the purpose to tune the value to keep original *Fc* of the EBI application.

2 AD5933+4E-AFE application customization: Once the values for each of the models have been obtained, the AD5933+4E-AFE was customized by adjusting the values of the following resistors: *Rrfb*, *R4* and applying (3.4) and (3.5).

From the AC Analysis:

$$V_{rfb}(t) = \frac{V_i(t)R_{tus}(t)R_{rfb}}{R_{cc1}R_4}\left(1 + \frac{50e3}{R_{G1}}\right) \quad \textbf{(3.4)}$$

From the DC Analysis:

$$V_{rfb} = \frac{V_{dd}}{2}\left(1 + \frac{R_{rfb}}{R_4}\right) - \frac{R_{rfb}}{R_4}V_{REF} \quad \textbf{(3.5)}$$

In order to make the most of the dynamic range of the ADC of the sensing stage of the AD5933, a DC bias voltage was introduced at the input with the value. Solving (3.6) for it was found that the values for *Rrfb* and *R4* and must be equal.

$$\frac{V_{dd}}{2} = \frac{V_{dd}}{2}\left(1 + \frac{R_{rfb}}{R_4}\right) - \frac{R_{rfb}}{R_4}V_{REF} \quad \textbf{(3.6)}$$

$$\frac{V_{dd}}{2}\ \frac{R_{rfb}}{R_4}V_{REF} = \frac{V_{dd}}{2}\ \frac{R_{rfb}}{R_4} \quad \textbf{(3.7)}$$

$$R_{rfb} = R_4 \quad \textbf{(3.8)}$$

$$V_{ref} = \frac{V_{dd}}{2} \quad \textbf{(3.9)}$$

By means of the AC analysis, an amplitude voltage at the input of the sensing stage of 1.5 Volts was applied and the resistance *RG1*, the gain resistance of INA111 on the 4E-AFE, was calculated with the Equation 3.10:

$$RG1 = \frac{50e3*2*V_i*R_{tus\_max}*R_{rfb}}{(V_{dd}*R_{cc1}*R_4)+(2*V_i*R_{tus\_max}*R_{rfb})} \quad \textbf{(3.10)}$$

From the analysis, it was obtained that several parameters have common values for all the EBI applications. The Table 3.2 lists the parameters with the corresponding values common for the EBI applications:

TABLE 3.2

Rcc1	Resistor of the voltage-current converter amplifier	7.5KΩ
R4	Resistor current-voltage	10 KΩ
Rrfb	Feedback resistor	10 KΩ
Vi	Vac injection	1.98V
Vdd	Vdc supply	3V

This way RG1 is the only parameter left that must be adjusted specifically to each application. Table 3.3 lists each of the obtained values for RG1 for each EBI application.

TABLE 3.3

APPLICATION	RG1(Ω)
TBC	6619
Arm-Arm	2851
Leg-Leg	3858
Trunk-Trunk	801
LC	654
RR	481

3.2.3 EBI Application Equivalent Spectroscopy Measurements

Hence, with the optimization of the system AD5933+4E-AFE already done, the impedance measurements for each model were made with both devices: the SFB7 and the AD5933+4E-AFE.

3.2.3.1. SFB7 measurements.

100 spectroscopy measurements have been taken in the frequency range from 3kHz to 1MHz for each of the equivalent circuits. Each obtained spectrum was saved in a text file, which contains the measurement frequency and both the measured resistance and reactance. The SFB7 distributes the measurement frequencies, exponentially distributing 256 measurement points between 3 kHz to 1 MHz. See Figure 3.12. This frequency distribution dedicates more measurement points to lower frequencies than for higher frequencies.

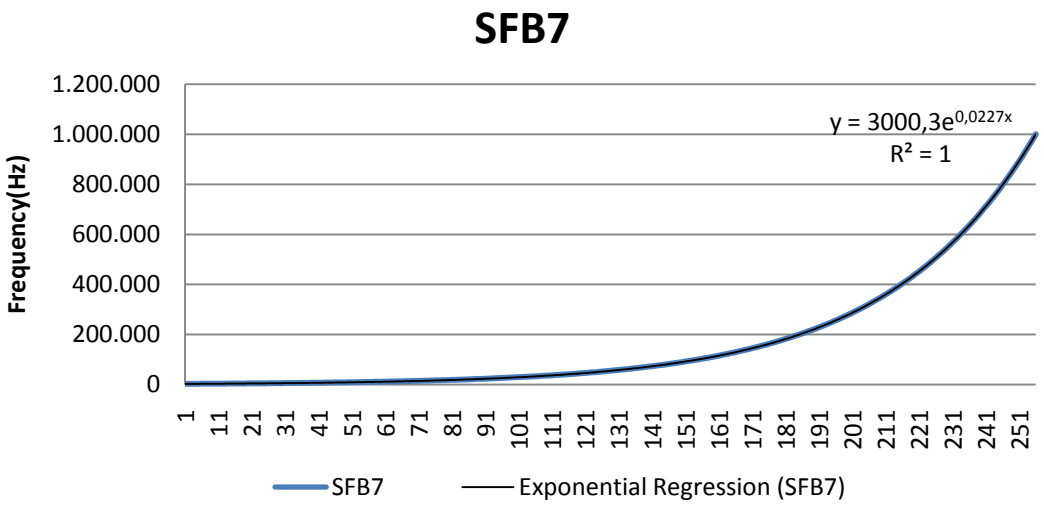

Figure 3.12 Frequency distribution of SFB7

3.2.3.2 AD5933+4-AFE measurements.

100 spectroscopy measurements have been taken in the frequency range from 3kHz to 100KHz. Each obtained spectrum was saved in a CSV file, which contains the measured frequencies, impedance, phase, resistance and reactance. AD5933 distributes the measurement frequencies lineally distribution 501 measurements points between 3kHz and 100KHz. See Figure 3.13. This frequency distribution dedicates the same number of point to high and low frequencies because the sample points are equidistant.

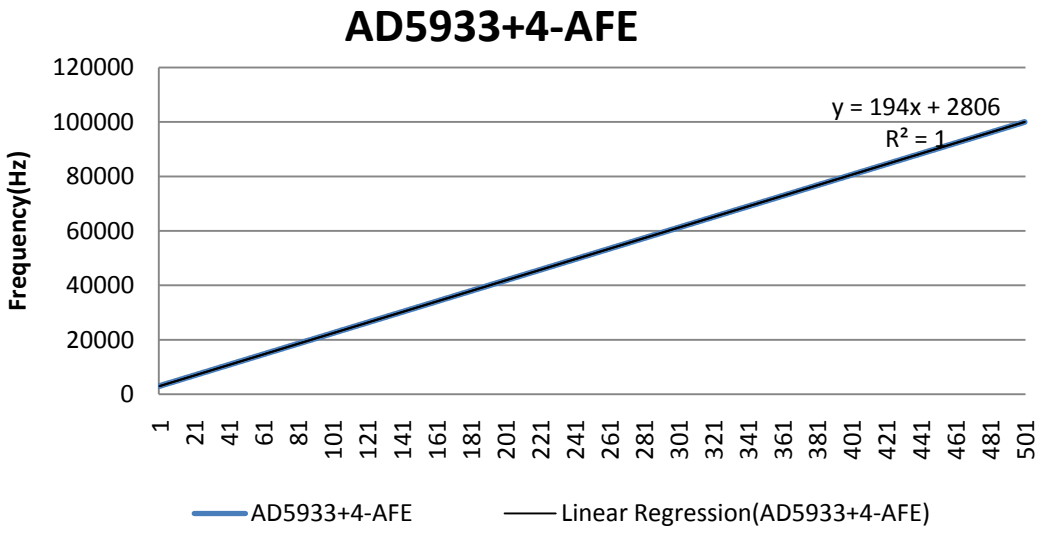

Figure 3.13 Frequency distribution of AD4933+4-AFE

All the obtained measurements, from both spectrometers, were processed with BioImp Software. In order to process the measurements taken by the AD5933+4E-AFE, a Matlab script was done in MATLAB to prepare the data files generated by the software controlling the AD5933+4E-AFE [31] to be imported by BioImp Software. In addition to the file conversion a specific file type definition was declared in BioImp to read the files as shown in Figure 3.14.

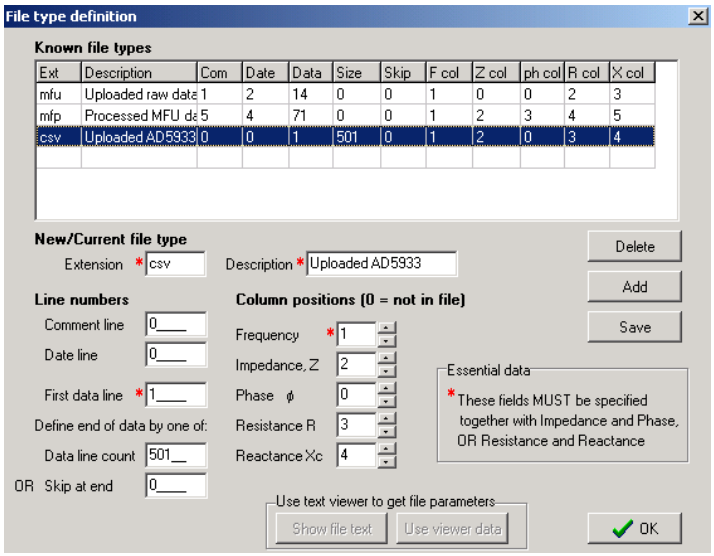

Figure 3.14 File definition Impedimed

3.2.4 Performance Comparison

The performance comparison was done based on the error obtained from the model parameters estimation, which was done from the impedance measurements from both systems, according to the work flow diagram showed in the Figure 3.15.

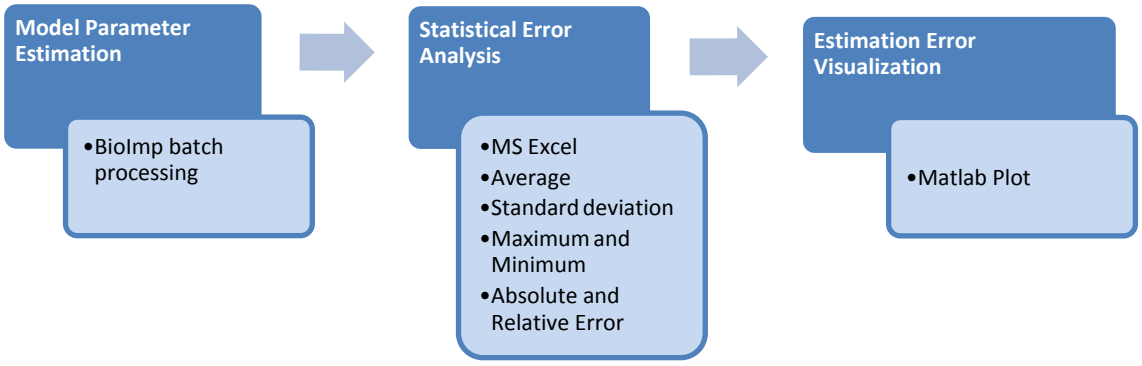

Fig 3.15 Performance comparison Process Overview

3.2.4.1 Model Parameter Estimation.

Once the files containing the 2R1C-models impedance measurements were uploaded into BioImp, the data files were batch processed to estimate the 2R1C parameters, see Figure 3.16. The estimation results from each measurement were saved into MS Excel format, see Figure 3.17. This way for each EBI application model two files containing the estimated parameters were obtained from the measurements taken with the SFB7 and the AD5933+4-AFE spectrometer.

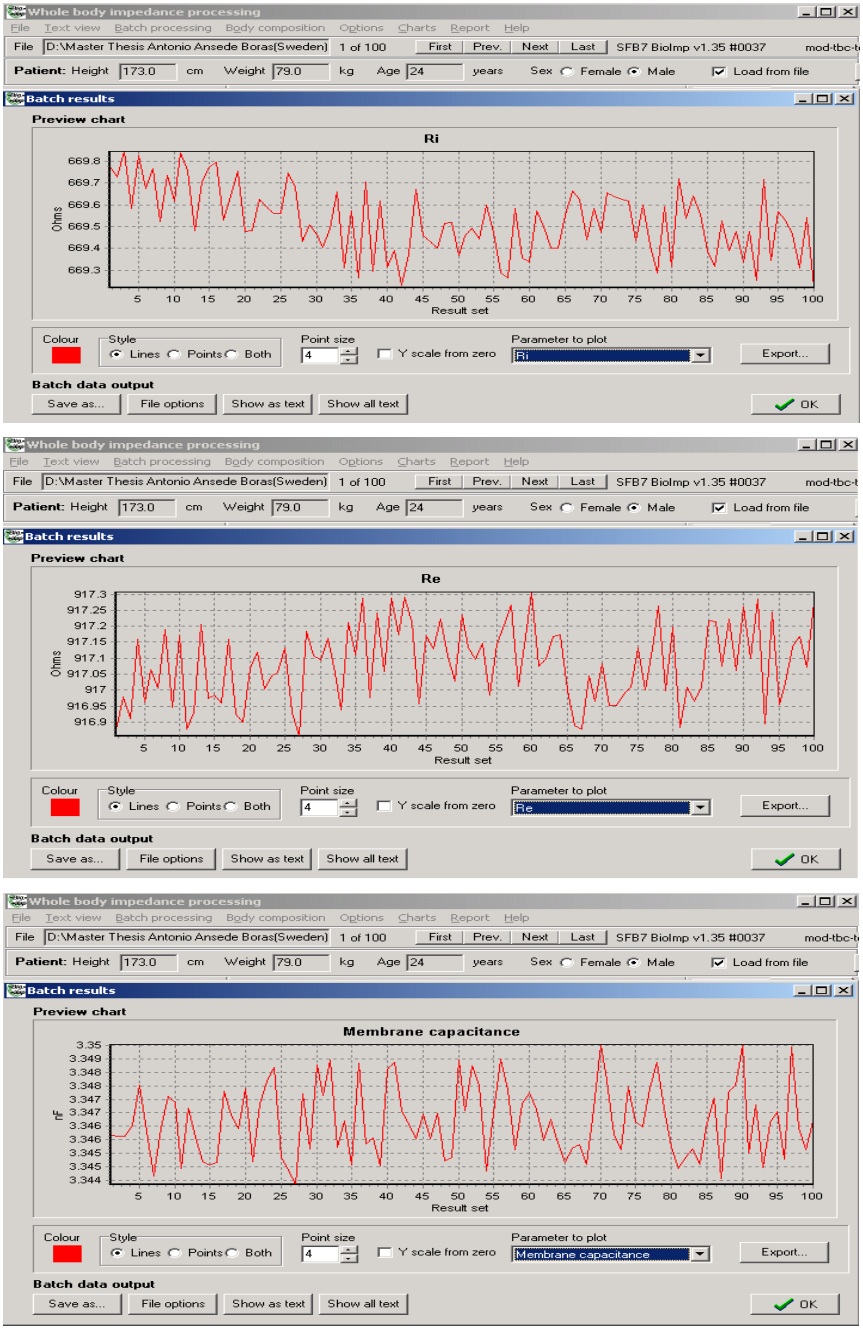

Figure 3.16 Batch results of *Ri, Re* and *Cm*

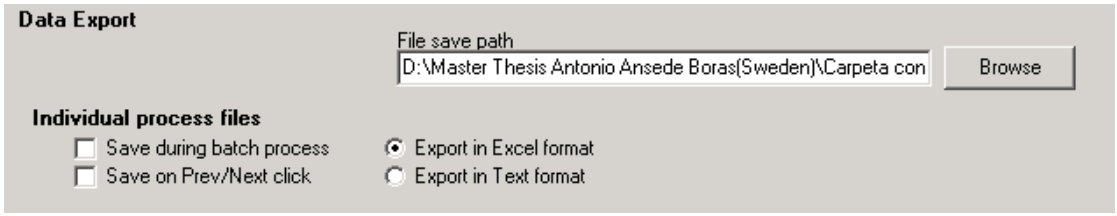

Figure 3.17 Data output file export options of BioImp

3.2.4.2 Statistics of the Model Parameter Estimation.

Each of the exported files from BioImp was processed with MS Excel to obtain the following statistical parameters from the values of *Re, Ri, Cm* and *Fc*:

- Average
- Standard deviation
- Maximum and Minimum
- Absolute and Relative Error

Note that the errors have been calculated comparing the estimated values with the real value of the passive components used to build the 2R1C.

3.2.4.3 Estimation Error Visualization.

To obtaine the plots with the comaprison results, the statistical values have been exported to a workspace of MatLab. Once in Matlab the average, maximum, minimum of the estimated values and the value of the component of each EBI model application have been plotted.

4.1 Overview

This chapter presents the results obtained from the measurements and the data analysis performed as described in the previous chapter. Firstly, the EBI spectroscopy measurements for each EBI application obtained with the SFB7 spectrometer will be shown by means of resistance and reactance spectra. Secondly, the values of the equivalent 2R1C models estimated from the initial obtained EBI spectroscopy measurements and the values of the implemented model will be listed in terms of R_e, R_i and C_m. Thirdly, the Impedance spectroscopy measurements taken from the implemented 2R1C-equivalent models with, both the SFB7 and AD5933+4-AFE, will be displayed represented as in the first point and finally, the comparison of both bioimpedance spectroscopy (BIS) devices will be shown with different statistical graphs.

4.2 SFB7 Measurements

In order to obtain an electrical circuit equivalent to the EBI measurement scenarios under study in this thesis work, experimental EBI Spectroscopy measurements have been taken and they are shown in the following graphs. The spectrum of the resistance and the reactance for each EBI scenario are plotted between in the frequency range 3 kHz to 1 MHz.

4.2.1 Total Body Composition (TBC):

In Figure 4.1 a) it is possible to observe that the maximum and minimum values of the resistance are approximately 600 Ω and 418 Ω respectively providing us with a dynamic range of approximately 182 Ω.

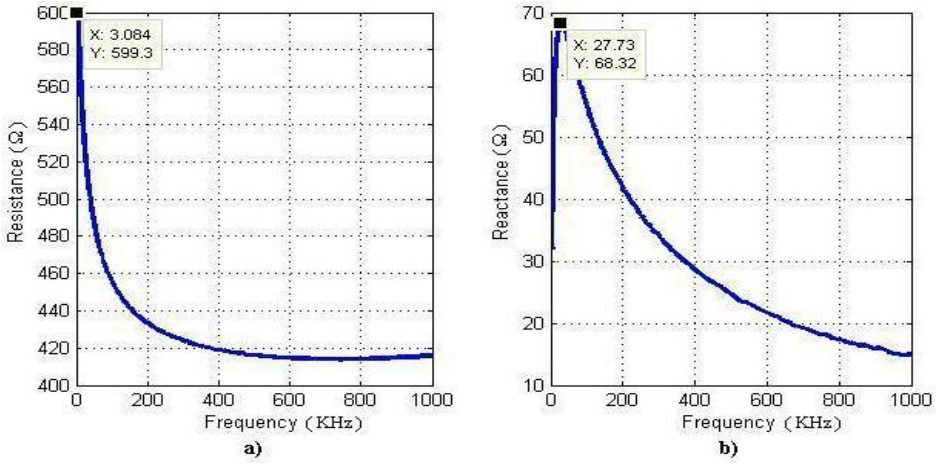

Figure 4.1 The spectra of the resistance and reactance are plotted respectively in a) and b). In b) it is possible to observe that there is only one dominant dispersion with a *Fc* value approximately of 28 kHz

4.2.2 Respiration Rate (RR):

In Figure 4.2 a) it is possible to observe that the maximum and minimum values of the resistance are approximately 37 Ω and 21 Ω respectively providing us with a dynamic range of approximately 16 Ω.

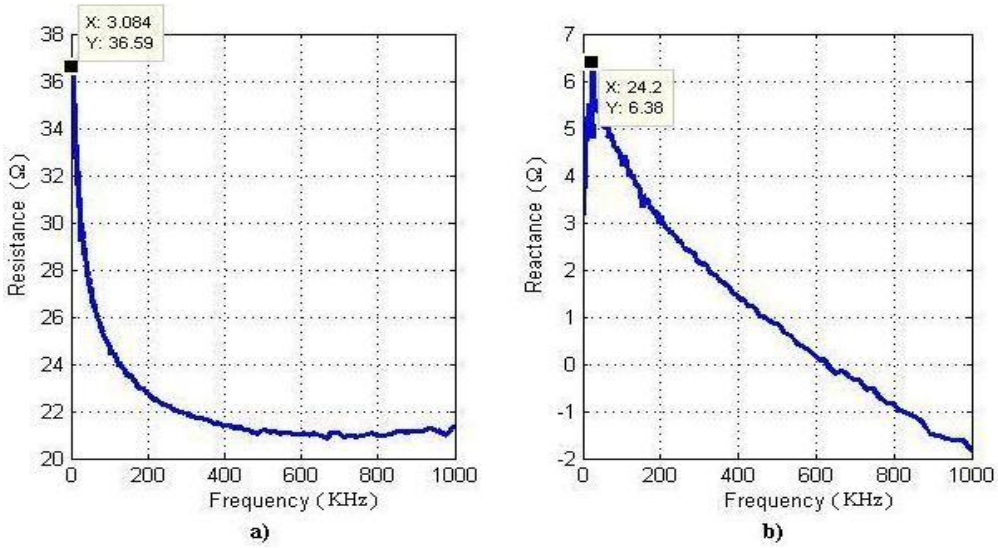

Figure 4.2 the spectra of the resistance and reactance are plotted respectively in a) and b). In b) it is possible to observe that there is only one dominant dispersion with a *Fc* value approximately of 24 kHz

4.2.3 Lungs Composition (LC):

In Figure 4.3 a) it is possible to observe that the maximum and minimum values of the resistance are approximately 50 Ω and 29 Ω respectively providing us with a dynamic range of approximately 21 Ω.

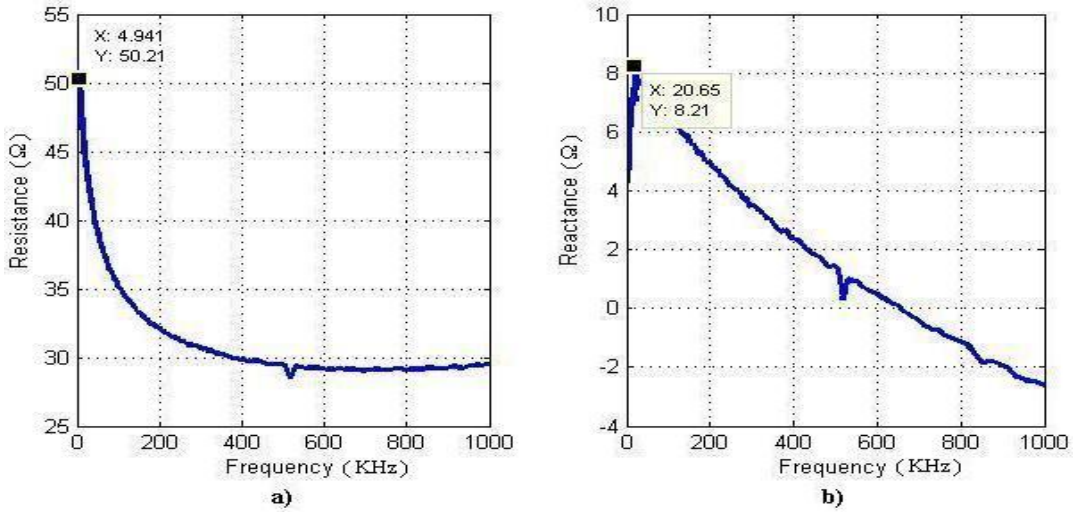

Figure 4.3 the spectra of the resistance and reactance are plotted respectively in a) and b). In b) it is possible to observe that there is only one dominant dispersion with a *Fc* value approximately of 21 kHz

4.2.4 Segmental Body Composition (SBC):

4.2.4.1 Arm-Arm (AA)

The effect observed at high frequencies, especially in the reactance, is consistent with the commonly known as Hook effect, which usually strongly affects measurements at frequencies above 500 kHz [32].

Despite the observed Hook Effect present in the EBI measurements, in Figure 4.4 b) it is possible to observe that the maximum and minimum values of the resistance are approximately 238 Ω and 170 Ω respectively providing us with a dynamic range of approximately 68 Ω.

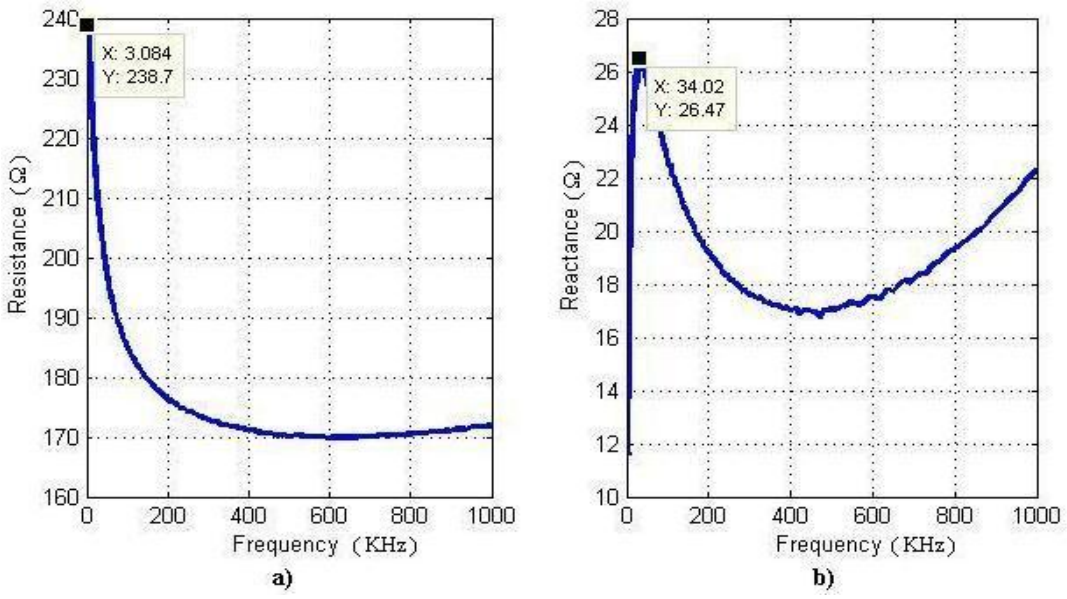

Figure 4.4 the spectra of the resistance and reactance are plotted respectively in a) and b). In b) besides to present a dispersion with a *Fc* value approximately of 34 kHz, it shows a second dominant dispersion at High frequencies.

4.2.4.2 Trunk-Trunk (TT):

Once again the hook effect can be observed at high frequencies in Figure 4.5, especially in the reactance in Figure 4.5 b). Nevertheless, in the spectrum of the resistance in Figure 4.5 a), it is possible to observe that the maximum and minimum values of the resistance are approximately 60 Ω and 38 Ω respectively providing us with a dynamic range of approximately 22 Ω.

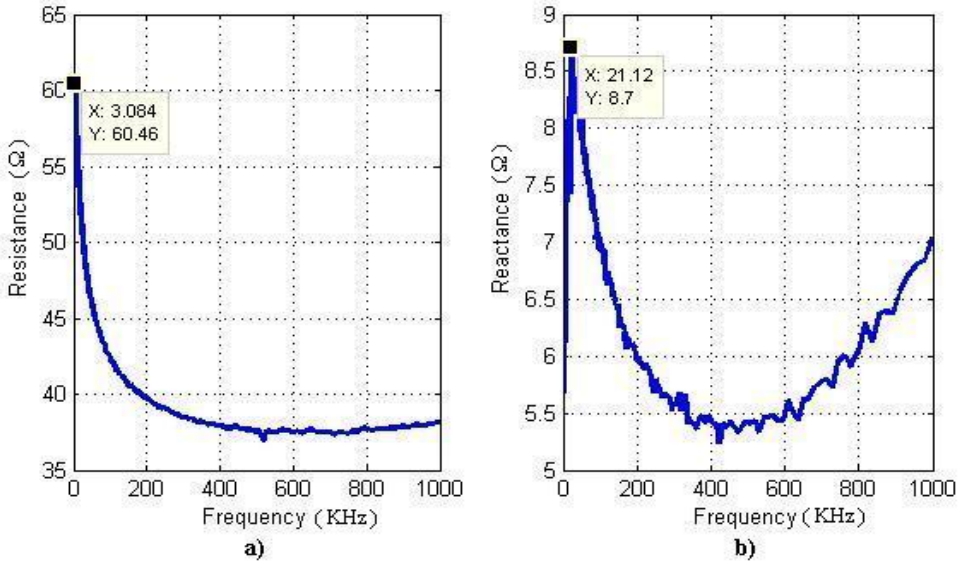

Figure 4.5 the spectra of the resistance and reactance are plotted respectively in a) and b). In b) besides to present a dispersion with a Fc value approximately of 21 kHz, it shows a second dominant dispersion at high frequencies.

4.2.4.3 Leg-Leg (LL):

In Figure 4.6 a) it is possible to observe that the maximum and minimum values of the resistance are approximately 328 Ω and 223 Ω respectively providing us with a dynamic range of approximately 105 Ω.

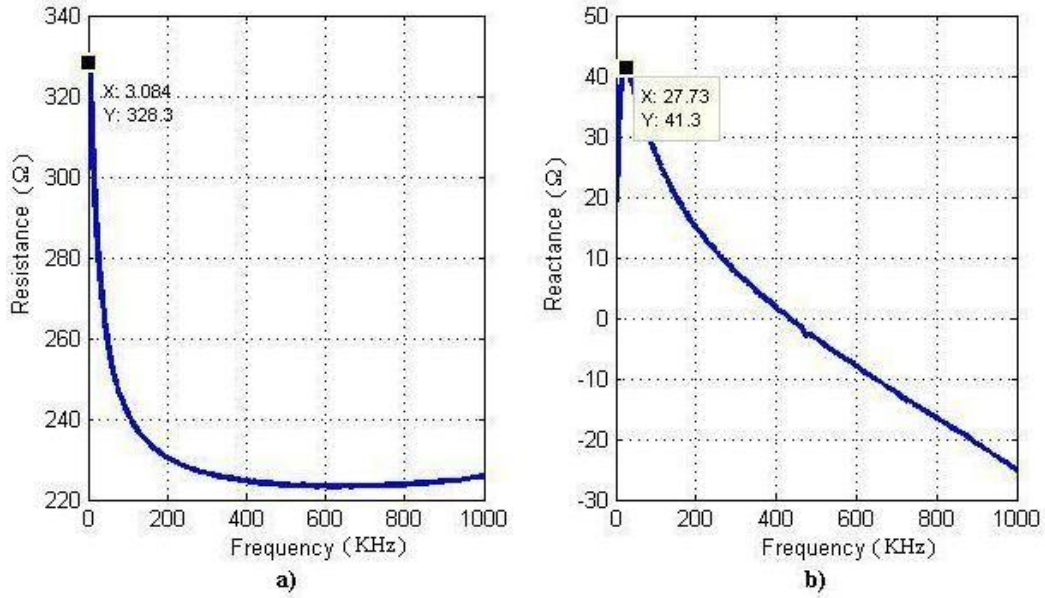

Figure 4.6 the spectra of the resistance and reactance are plotted respectively in a) and b). In b) it is possible to observe that there is only one dominant dispersion with a Fc value approximately of 28 kHz

4.2.1. Measurements Summary

The obtained spectroscopy EBI measurements present a resistance and a reactance with a strong frequency dependency. The dynamic range of impedance values for both resistance and reactance is listed below.

TABLE 4.1 REACTANCE AND RESISTANCE RANGE PER APPLICATION

Applications	Rmax	Rmin	Xcmax	Xcmin
TBC	600	412	68.81	11.98
RR	40.54	20.1	6.87	-2.6
LC	54.18	25.3	8.85	-2.95
AA	241.2	168.4	26.91	10.81
TT	61.46	36.53	9.73	4.7
LL	333.89	222.35	42.99	-25.85

4.3 Modeling 2R1C

After processing all the EBI measurements obtained for each application with the batch processing tool of the BioImp software and averaging the results, the values for the parameters of the 2R1C-equivalent circuit model and the characteristic frequency for each application have been obtained. The values are listed in Table 4.2

TABLE 4.2. RE, RI, CM AND FC PER APPLICATION

Applications	Re(Ω)	Ri(Ω)	Cm(nF)	Fc(KHz)
TBC	622	1149.5	2.99	30.1
RR	39.6	41.5	77.1	25.5
LC	54	50.5	46.2	33.0
AA	246.5	477.9	6.37	34.5
TT	66.4	67.1	46.5	25.6
LL	340.8	633.9	6.61	25.3

The load dynamic range has been enlarged to increase the applicability of the working models to more subjects. Therefore the components of the 2R1C-equivalent circuit have been re-calculated according to the process previously explained in section 3.2 and the newly obtained theoretical values are listed in the Table 4.3:

TABLE 4.3 THEORETICAL VALUES OF THE 2R1C COMPONENTS

Application	Re(Ω)	Cm(nF)	Fc(KHz)	Ri(Ω)
TBC	933	2.99	30.1	835
RR	59.4	77.1	25.5	21.5
LC	81	46.2	33	23.4
AA	369.75	6.37	34.5	354
TT	99.6	46.5	25.6	34
LL	511.2	6.61	25.3	440

The circuit was implemented using an E-24 series resistor for *Re*, a potentiometer for *Ri* and a MKT370 (Vishay BC) series capacitor for *Cm*. The values for the circuit components were adjusted to the experimental values of *Re* and *Cm* trimming the potentiometer *Ri*, this way obtaining the final values for the 2R1C components. See Table 4.4.

TABLE 4.4 FINAL VALUES OF THE 2R1C COMPONENTS

Application	Re(Ω)	Cm(nF)	Fc(KHz)	Ri(Ω)
TBC	917.5	3.42	30.1	629
RR	58.5	75.7	25.5	23.9
LC	81.5	47.7	33	19.6
AA	364.6	6.20	34.5	379
TT	99	44	25.6	42.3
LL	510	6.55	25.3	450

4.4. Spectroscopy Measurements in 2R1C Models

Once the equivalents electrical circuits and the optimization of AD5933+4E-AFE have been already done, the impedance measurements for each model were made by both, the device SFB7 and the AD5933+4E-AFE. The obtained measurements with each of the spectrometers for each application are shown in the follow figures.

4.4.1 TBC:

Figure 4.7 contains the plots of the reactance and resistance spectrum of the TBC application obtained from the SFB7 and AD5993+4-AFE. In the resistance spectrum it is possible to observe that the maximum and minimum values are approximately 900 Ω and 390 Ω respectively, providing us with a dynamic range of approximately 510 Ω. As the graphs denote the curves, resistance and reactance for both devices are overlapped, which means that the measurements of SFB7 and AD5933+4-AFE are very similar. It is also possible to observe that at low frequencies, between 3kHz and 6KHz, the device AD5933+4-AFE produce certain dispersion on the measurement.

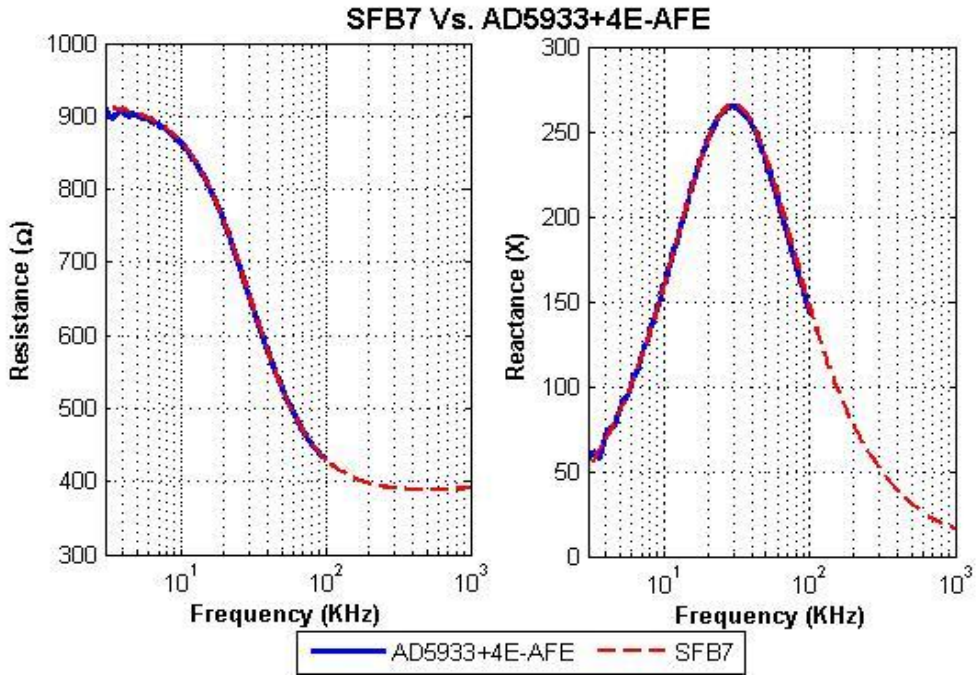

Figure 4.7 the left part of the figure the spectra resistance and the right part the spectra reactance are plotted measured from, SFB7 and AD5993+4-AFE. In the reactance is possible to observe that there is only one dominant dispersion with a Fc value approximately of 30 kHz

4.4.2 RR:

In Figure 4.8 the reactance and resistance spectra of the TBC application for SFB7 and AD5993+4-AFE are plotted. In the resistance curve is possible to observe that the maximum and minimum values are approximately 57 Ω and 16 Ω respectively, providing us with a dynamic range of approximately 41 Ω. As the graphs denote the curves, resistance and reactance for the both devices are overlapped, therefore it means that the measurements of SFB7 and AD5933+4-AFE are very similar. It is also possible to observe that at low frequencies, between 3kHz and 6KHz, the measurements performed with the device AD5933+4-AFE present a dispersion.

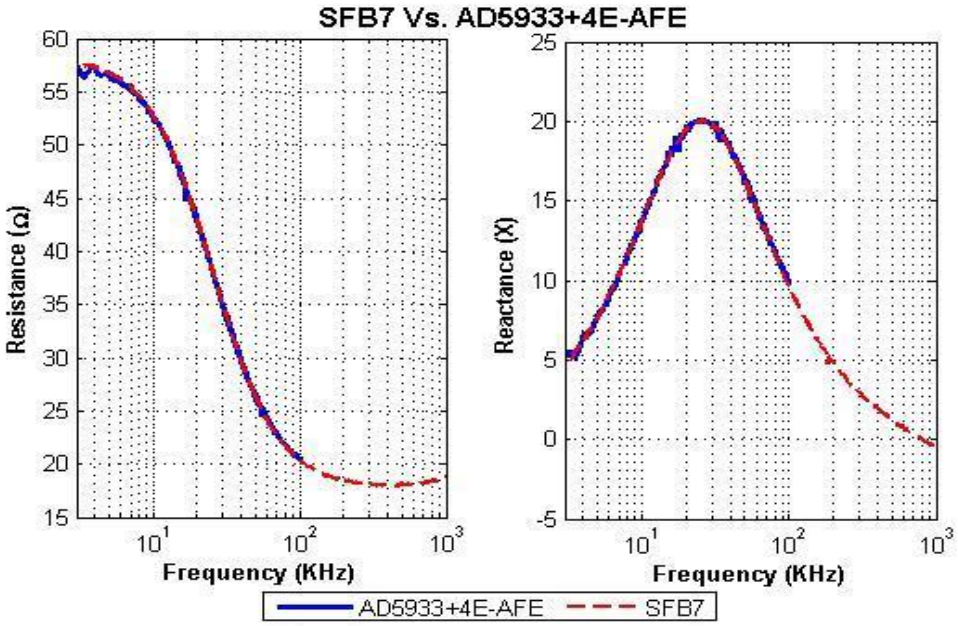

Figure 4.8 the left part of the figure the spectra resistance and the right part the spectra reactance are plotted measured from both, SFB7 and AD5993+4-AFE. In the reactance is possible to observe that there is only one dominant dispersion with a *Fc* value approximately of 27 kHz

4.4.3 LC:

In Figure 4.9 the reactance and resistance spectra of the TBC application for SFB7 and AD5993+4-AFE are plotted. In the resistance curve is possible to observe that the maximum and minimum values are approximately 80 Ω and 18 Ω respectively, providing us with a dynamic range of approximately 62 Ω. As the graphs denote the curves, resistance and reactance for the both devices are overlapped, therefore it means that the measurements of SFB7 and AD5933+4-AFE are very similar. It is also possible to observe that at low frequencies, between 3KHz and 6KHz, the measurements performed with the device AD5933+4-AFE present a dispersion.

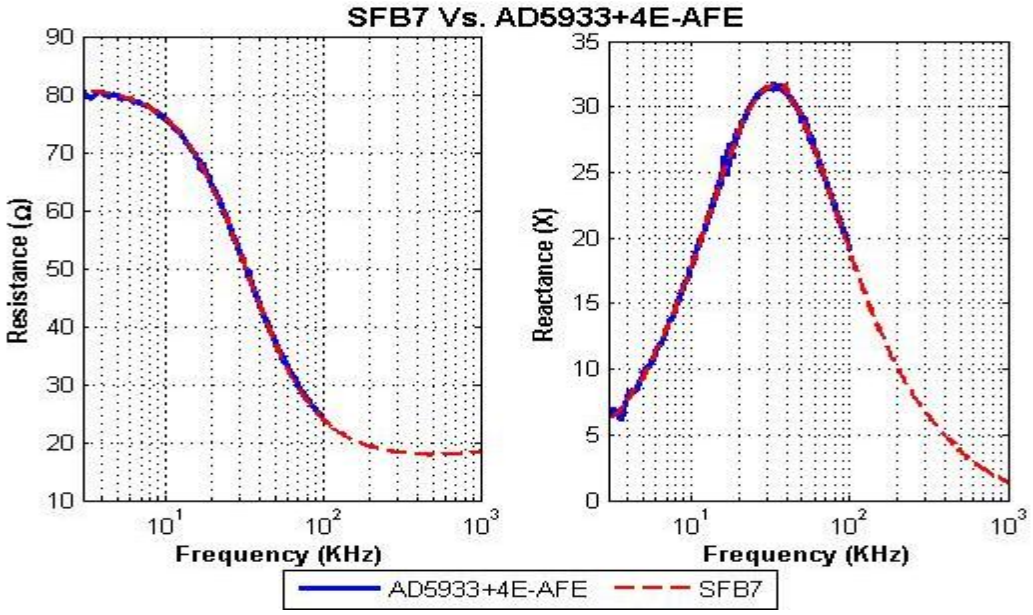

Figure 4.9 the left part of the figure the spectra resistance and the right part the spectra reactance are plotted measured from both, SFB7 and AD5993+4-AFE. In the reactance is possible to observe that there is only one dominant dispersion with a *Fc* value approximately of 35 kHz

4.4.4 AA:

In the Figure 4.10 is plotted the reactance and resistance of the TBC application for SFB7 and AD5993+4-AFE.

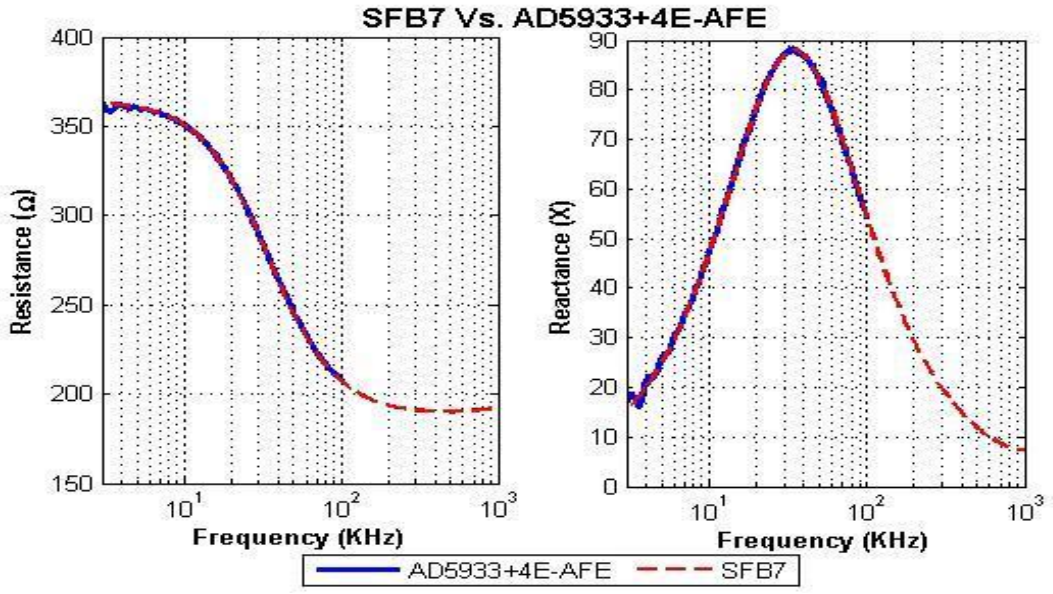

Figure 4.10 the left part of the figure the spectra resistance and the right part the spectra reactance are plotted measured from both, SFB7 and AD5993+4-AFE. In the reactance is possible to observe that there is only one dominant dispersion with a *Fc* value approximately of 35 kHz

In the resistance curve is possible to observe that the maximum and minimum values are approximately 365 Ω and 185 Ω respectively, providing us with a dynamic range of approximately 180 Ω. As the graphs denote the curves, resistance and reactance for the both devices are overlapped; therefore it means that the measurements of SFB7 and AD5933+4-AFE are very similar. It is also possible to observe that at low frequencies, between 3kHz and 6KHz, the measurements performed with the device AD5933+4-AFE present a dispersion.

4.4.5 LL:

In the Figure 4.11 is plotted the reactance and resistance of the TBC application for SFB7 and AD5993+4-AFE. In the resistance curve is possible to observe that the maximum and minimum values are approximately 500 Ω and 240 Ω respectively, providing us with a dynamic range of approximately 260 Ω. As the graphs denote the curves, resistance and reactance for the both devices are overlapped; therefore it means that the measurements of SFB7 and AD5933+4-AFE are very similar. It is also possible to observe that at low frequencies, between 3KHz and 6KHz, the measurements performed with the device AD5933+4-AFE present a dispersion.

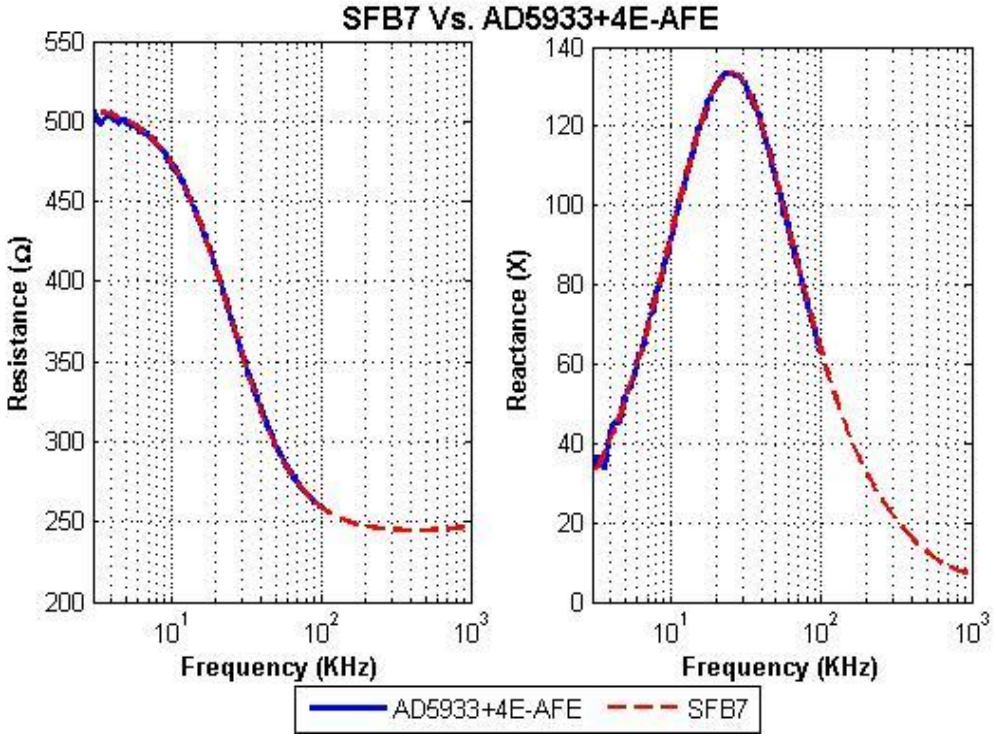

Figure 4.11 the left part of the figure the spectra resistance and the right part the spectra reactance are plotted measured from both, SFB7 and AD5993+4-AFE. In the reactance is possible to observe that there is only one dominant dispersion with a *Fc* value approximately of 25 kHz

4.4.6 TT:

In the Figure 4.12 is plotted the reactance and resistance of the TBC application for SFB7 and AD5993+4-AFE.

TABLE 4.5 THEORETICAL VALUES 2R1C COMPONENTS

Application	*Re*(Ω)	*Ri*(Ω)	*Cm*(nF)	*Fc*(kHz)
TBC	933	835	2.99	30.1
RR	59.4	21.5	77.1	25.5
LC	81	23.4	46.2	33
AA	369.75	354	6.37	34.5
TT	99.6	34	46.5	25.6
LL	511.2	440	6.61	25.3

In the resistance curve is possible to observe that the maximum and minimum values are approximately 98 Ω and 31 Ω respectively, providing us with a dynamic range of approximately 67 Ω. As the graphs denote the curves, resistance and reactance for the both devices are overlapped, therefore it means that the measurements of SFB7 and AD5933+4-AFE are very similar. It is also possible to observe that at low frequencies, between 3kHz and 6kHz, the measurements performed with the device AD5933+4-AFE present a dispersion.

4.4.7 Comparison among the Theoretical Model Values and the Estimated Model Values

With one of the measurements taken by each device, SFB7 and AD5933 +4- AFE, and once the data were processed with BioImp software to obtain the value of *Re*, *Ri*, *Cm* and *Fc* then Figure 4.13 has been produced. It shows the comparison between the estimated model values *Re*, *Ri*, *Cm* and the characteristic frequency *Fc* obtained for each application and device with the theoretical measured values, which are enlisted in Table 4.5.

In Figure 4.13 it is possible to observe the calculated value and the obtained value from the measurements of both devices are quite similar, the maximum difference is in the value of *Ri*, between the calculated value and obtained value from the devices in the TBC application.

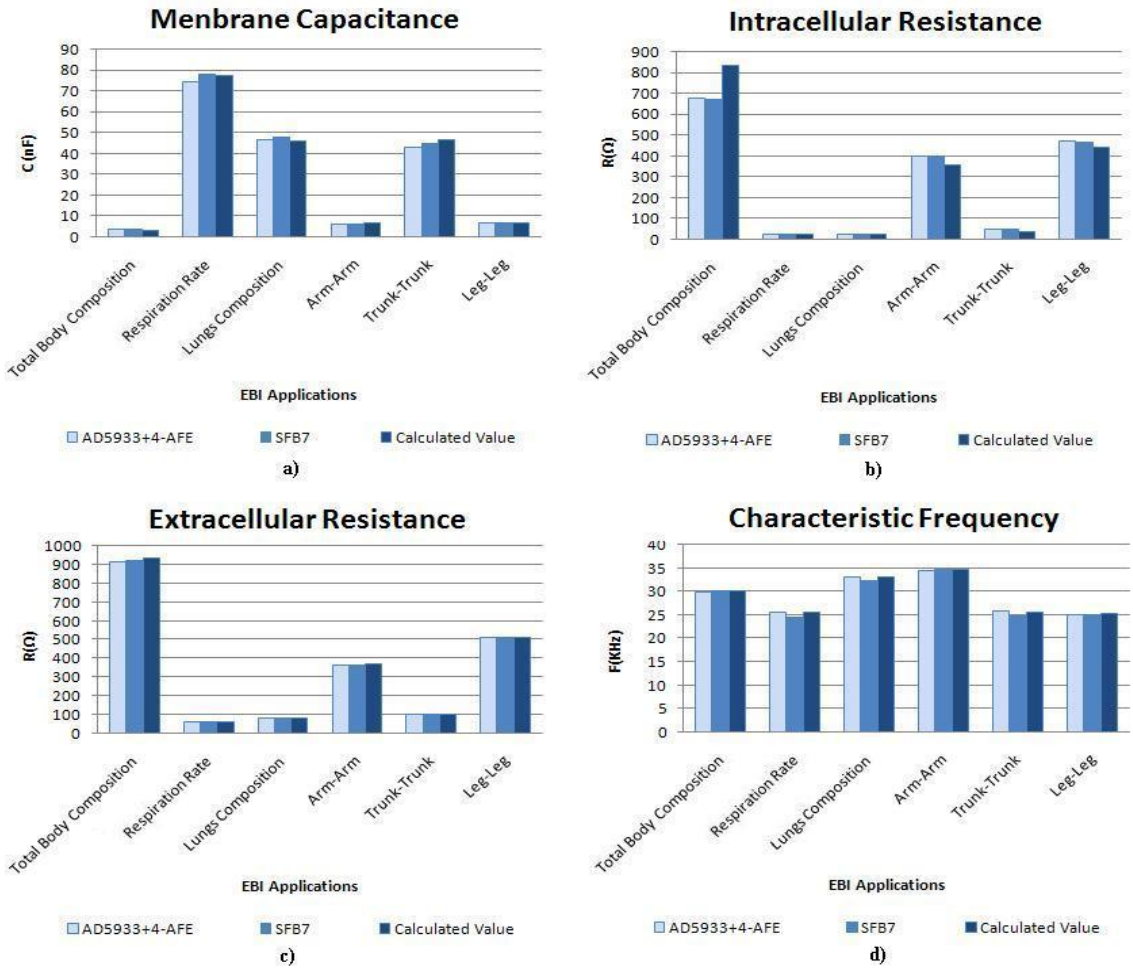

Figure 4.13 This graph shows in a) the membrane capacitance, in b) the intracellular resistance, in c) the extracellular Resistance and in d) the characteristic frequency per each application and measured with, both devices the SFB7 and AD5933+4-AFE, and also the theoretical value calculated.

4.5. SFB7 Vs. AD5933+4-AFE

In order to show the performance comparison between the SFB7 and the AD5933+4-AFE the following statistical parameters were chosen:

- Absolute and Relative Error
- Average
- Standard deviation
- Maximum and Minimum

Therefore, with all the measurements already processed with BioImp software, all the estimation results were exported to a MS Excel file. Once all the data were exported to MS Excel, the statistical values were calculated with the statistical tools available within MS Excel. Firstly, the absolute and relative error comparisons between SFB7 and AD5933+4-AFE were done. Figure 4.14 and 4.15 show both errors.

Figure 4.14 Relative error of *Ri, Re, Cm* and *Fc* for each application and device: SFB7 and AD5933+4-AFE.

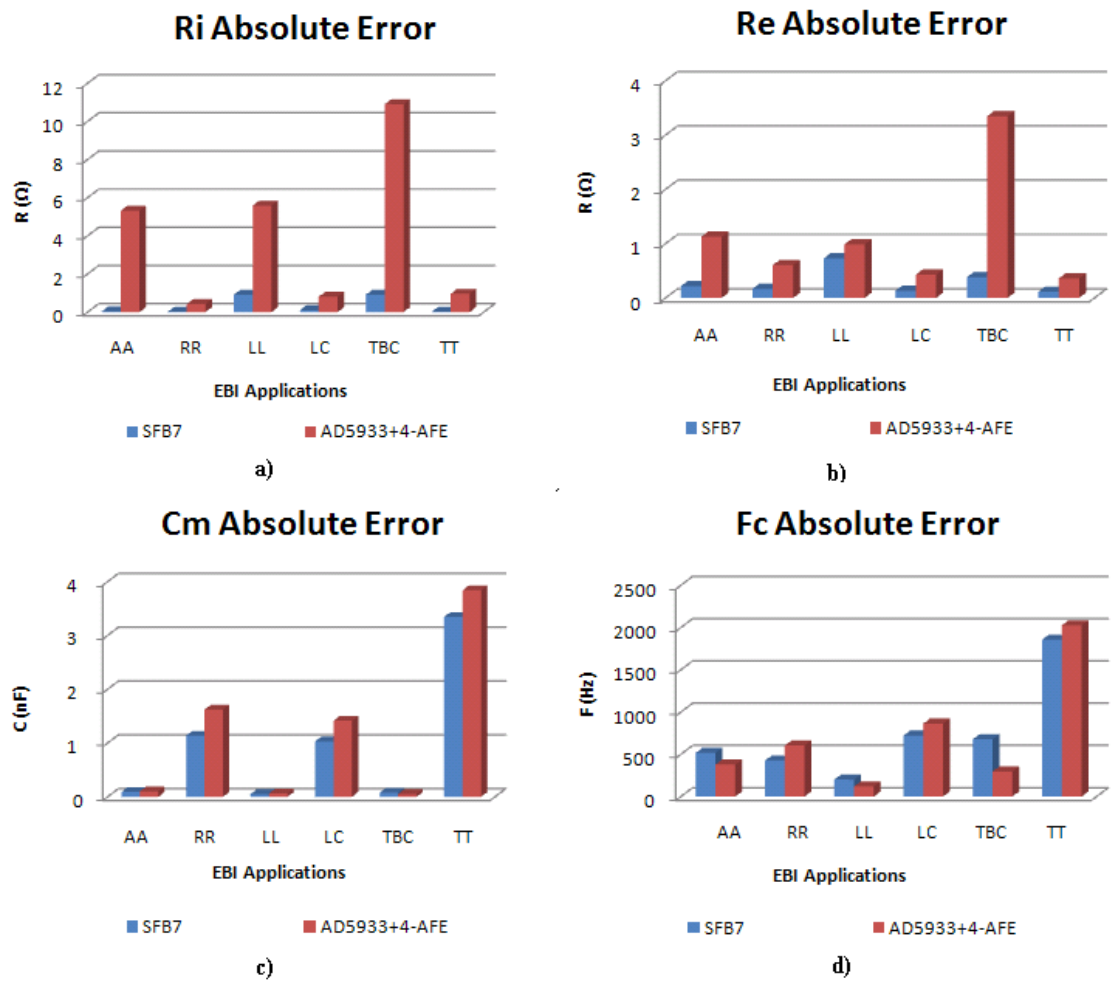

Fig 4.15 Absolute error of *Ri, Re, Cm* and *Fc* per each application and device (SFB7 and AD5933+4-AFE)

As it is possible to see in Figure 4.14 in all the calculated values for each application the relative error produced by the AD5933+4-AFE is slightly bigger than the produced by the SFB7. The maximum relative error with regarding to the real value of each parameter is about of 8% and it occurs in the TT application, also the average value of the relative error is approximately around 2%.

The absolute error per application and circuital value of the used model is shown in Figure 4.15 and it was shown in the case of the relative error but in the respective units that the error obtained with the AD5933+4-AFE is larger than the error obtained with the SFB7. The maximum absolute error in the case of the calculated value from the impedance measurements is for the resistors about 10 Ω, for the capacitor about 4pF and for Fc is 2kHz

Secondly, the standard deviation was calculated also with MS Excel. Figure 4.16 shows the comparison of the standard deviation obtained with each of the devices.

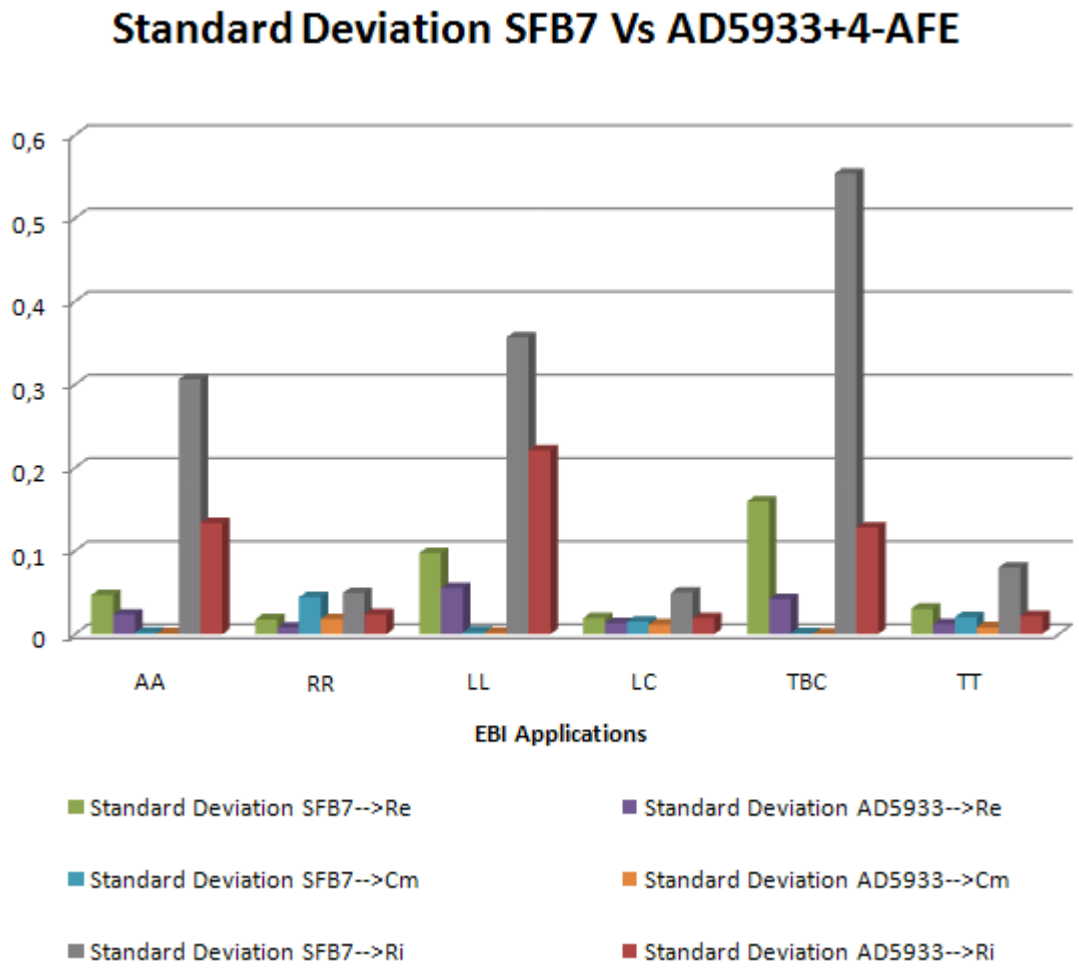

Figure 4.16 Standard deviation of *Ri, Re, Cm* for each application and impedance spectrometer device: SFB7 and AD5933+4-AFE.

Although the relative error obtained with the AD5933+4-AFE is most of the time larger than the error obtained with the SFB7, as shown in Figure 4.15, the standard deviation of the SFB7 is larger than the standard deviation produced by the AD5933+4-AFE in all the circuital values calculated in each of the applications.

Finally in Matlab, the average, maximum, minimum of the estimated values and the real value of the component of each EBI model application have been plotted on Figures 4.17, 4.18, 4.19, 4.20, 4.21 and 4.22.

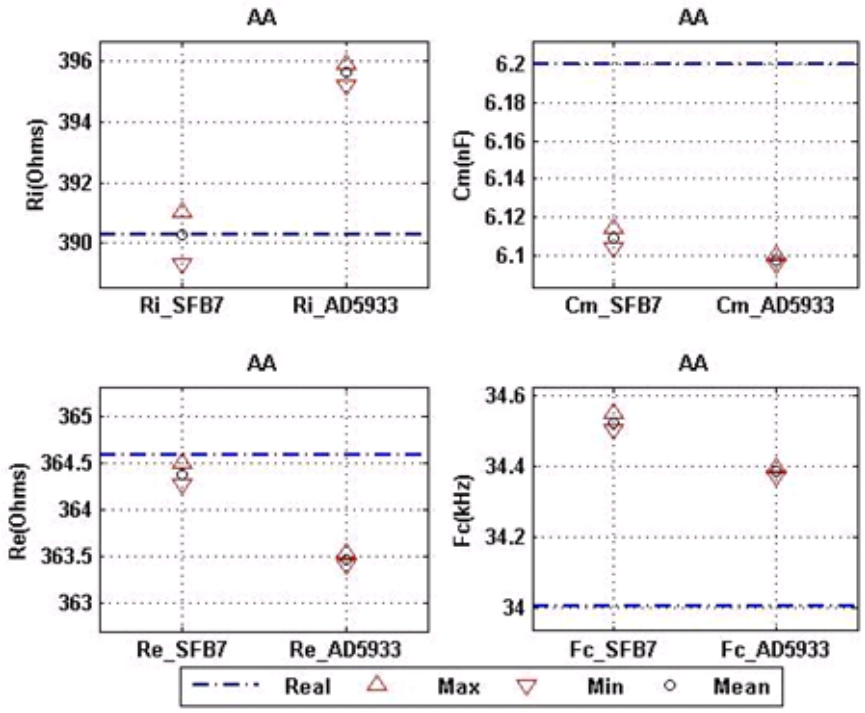

Figure 4.17 the maximum, minimum, average and real values of the 2R1C model (*Re, Ri and Cm*) and the characteristic frequency (*Fc*) for the segmental body composition Arm-Arm application.

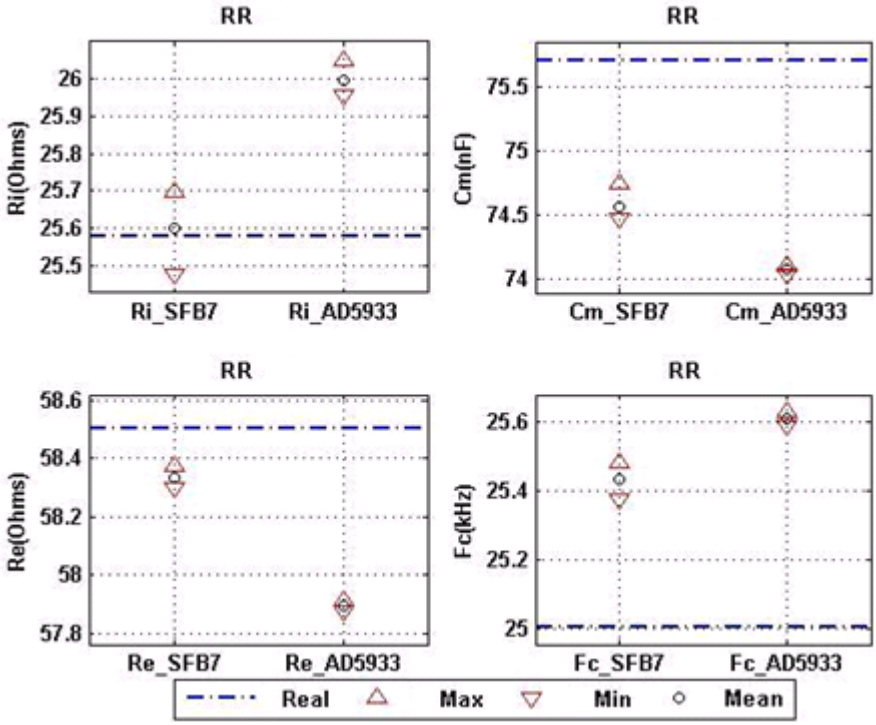

Figure 4.18 the maximum, minimum, average and real values of the 2R1C model (*Re, Ri and Cm*) and the characteristic frequency (*Fc*) for the Respiration Rate application.

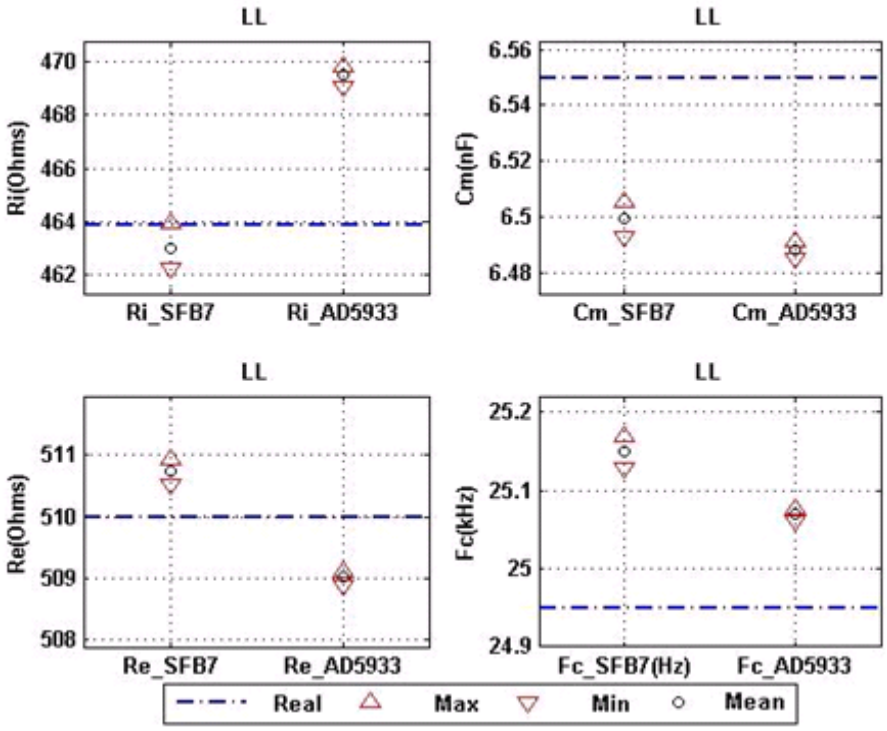

Figure 4.19 the maximum, minimum, average and real values of the 2R1C model (Re, Ri and Cm) and the characteristic frequency (*Fc*) for the segmental body composition Leg-Leg Application.

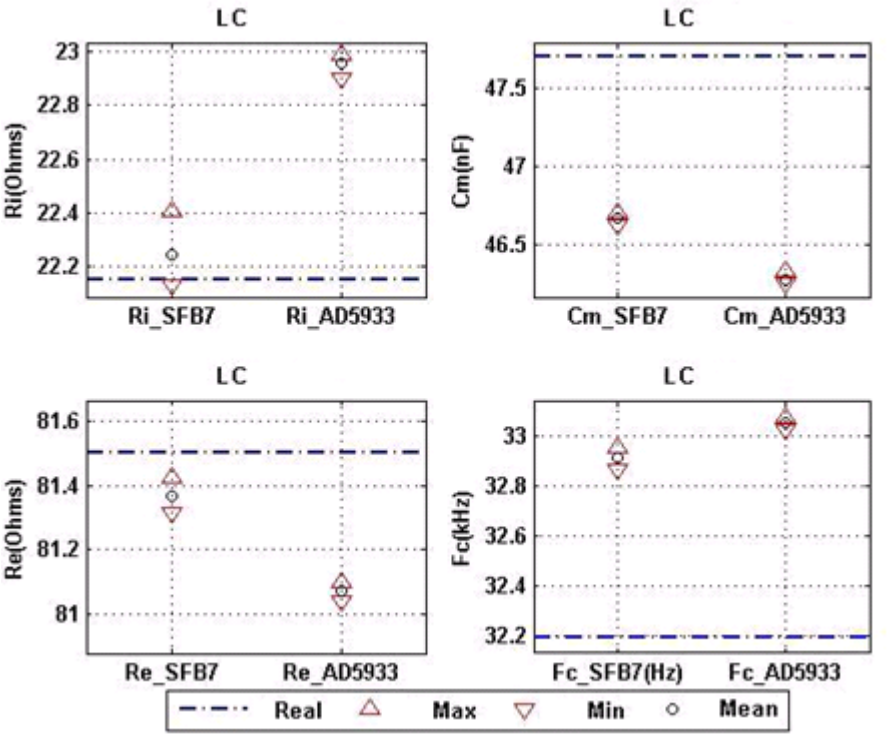

Figure 4.20 the maximum, minimum, average and real values of the 2R1C model (*Re, Ri and Cm*) and the characteristic frequency (*Fc*) for the Lungs Composition application.

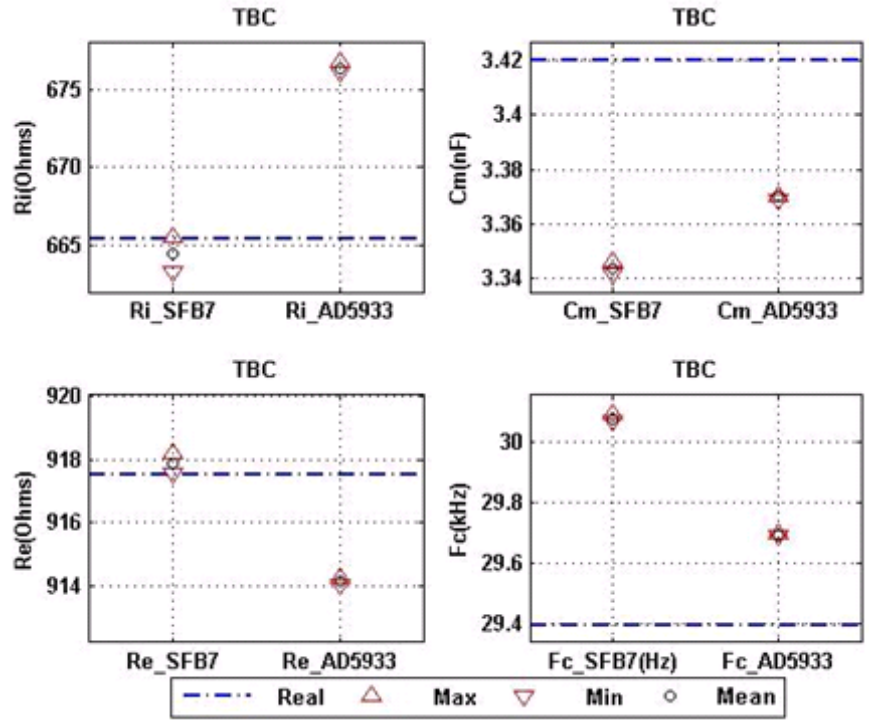

Figure 4.21 the maximum, minimum, average and real values of the 2R1C model (*Re, Ri and Cm*) and the characteristic frequency (*Fc*) for the Total Body Composition application.

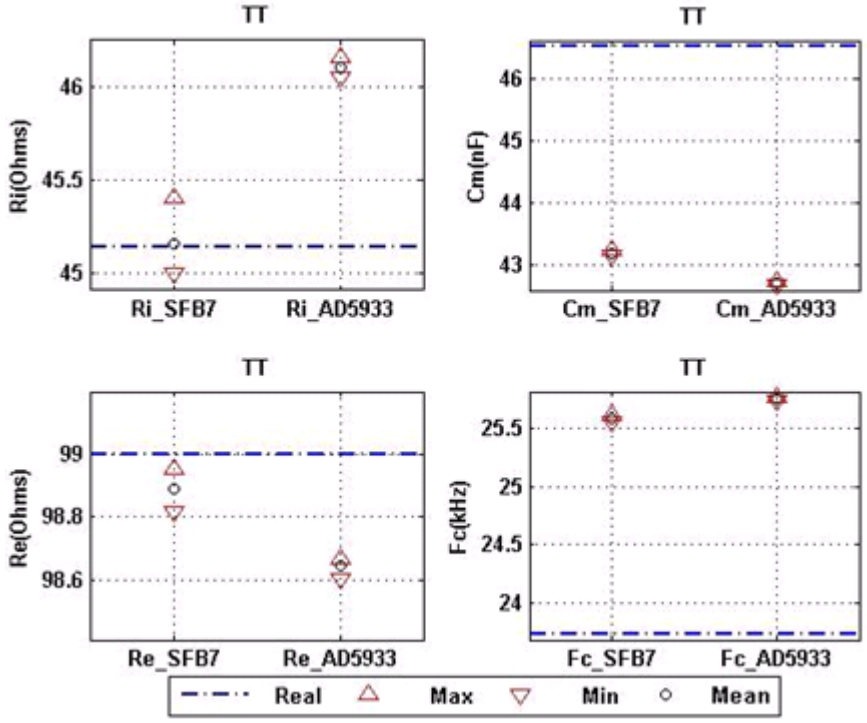

Figure 4.22 the maximum, minimum, average and real values of the 2R1C model (*Re, Ri and Cm*) and the characteristic frequency (*Fc*) for the segmental body composition Trunk-Trunk application.

The previous figures show the maximum, minimum, average and real values for the 2R1C model and it is possible to see that in almost in all the EBI applications, the SFB7 produces a closer value to the real values of the of the 2R1C models than the values estimated with the AD5933+4-AFE measurements, as shown in Figure 4.14 and Figure 4.15, the relative error and the absolute error respectively. In addition the Figures show with the indicators of the maximums and minimums that the dispersion of estimations produced by the SFB7 measurements is larger than the estimations produced with the AD5933+4-AFE measurements as shown in Figure 4.16.

5.1. Performance of 2R1C Components Estimation

Although experimental EBI measurements were used to obtain the values of the components of the 2R1C models. The values of the bridge resistors were adjusted with α parameter in order to consider the variance in the morphology of the population like size, weight, complexion etc. Nevertheless the α parameter was chosen arbitrarily modifying all the models. Therefore, in order to improve this step of the parameters estimation a target study should be realized in several subjects to reach a better approximation to an α parameter in an empiric way.

5.2. Study of Errors: Relative Error and Standard Deviation

Table 5.1 and Table 5.2 show respectively the relative error and the standard deviation of the devices SFB7 and AD5933. Therefore according to the theoretic definition of accuracy and precision and with the dates from tables, it is possible to affirm that the device SFB7 has a better accuracy than AD5933 due to its low relative error with real values and the AD5933 has a better preciseness than SFB7 because of the exhibited low standard deviation.

TABLE 5.1 RELATIVE ERROR: SFB7 VS. AD5933+4-AFE

SFB7/AD5933	**Ri**		**Cm**		**Re**		**Fc**	
AA	0.01%	1.36%	1.47%	1.65%	0.06%	0.31%	1.52%	1.11%
RR	0.08%	1.63%	1.50%	2.14%	0.29%	1.03%	1.70%	2.42%
LL	0.20%	1.20%	0.78%	0.94%	0.14%	0.19%	0.80%	0.48%
LC	0.44%	3.63%	2.16%	2.97%	0.16%	0.53%	2.24%	2.68%
TBC	0.14%	1.64%	2.22%	1.47%	0.04%	0.36%	2.31%	1.01%
TT	0.04%	2.13%	7.19%	8.25%	0.11%	0.36%	7.82%	8.54%

TABLE 5.2 STANDARD DEVIATION: SFB7 VS. AD5933+4-AFE

SFB7/AD5933	Ri		Cm		Re		Fc	
AA	3.06E-01	1.33E-01	1.88E-03	9.57E-04	4.71E-02	2.35E-02	7.56E-03	5.15E-03
RR	4.93E-02	2.38E-02	4.44E-02	1.81E-02	1.77E-02	7.70E-03	1.79E-02	8.54E-03
LL	3.57E-01	2.21E-01	2.66E-03	1.92E-03	9.77E-02	5.55E-02	7.80E-03	3.27E-03
LC	4.98E-02	1.93E-02	1.49E-02	1.17E-02	1.93E-02	1.31E-02	1.54E-02	8.76E-03
TBC	5.54E-01	1.28E-01	9.15E-04	3.05E-04	1.59E-01	4.23E-02	5.32E-03	2.17E-03
TT	7.99E-02	2.17E-02	2.03E-02	8.11E-03	3.04E-02	1.22E-02	1.26E-02	5.25E-03

"The accuracy is the degree of closeness of a measured or calculated quantity to its actual true value" [33], while Precision or Preciseness the quality of being reproducible in amount or performance.

Given the large amount of obtained data and according to Table 5.1, Table 5.3 was made as summary of the worst case of error per application and device. It has made adding the square of the relative error obtained for every circuit parameter per each EBI application.

TABLE 5.3 QUADRATIC ADDITION

Application	SFB7	
AA	2.11%	2.43%
RR	2.29%	3.76%
LL	1.14%	1.61%
LC	3.15%	5.43%
TBC	3.21%	2.45%
TT	10.62%	12.07%

Taking into account Table 5.3, the device SFB7 has exhibited a lower error in the estimation of the circuit parameters of model 2R1C in almost all the EBI application, except in the application Total Body Composition, in which the AD5933+4-AFE has a 0.76% less of error than the SFB7. The higher difference between both devices is in the Lungs Composition application, with 2.28% and the highest error in both systems are in the application Trunk-Trunk.

In order to decide for which applications the AD5933+4-AFE is more suitable to use, we have focused in error in medical applications attending to the following expression:

Measurement Error < Estimator Error < Application Error

On one hand, in the measurement of lungs circulate air volume [34] [35] the error measured with a neumotacometer and with EIT is around 20%, then the application error is almost two times higher (12%) than the worse EBI application error studied in this work. On the other hand, in peritoneal dialysis [36] using the impedance parameter R normalized by body height H for the right-side (R_{RS}/H) versus mean blood pressure (BP_{MEAN}), the standard deviation for unstable and stable patients is 4.90 ± 2.87 and 8.19 ± 2.26, respectively. Consequently the data are spread out over the average with maximums errors around 58% and 28%, respectively.

Therefore is possible to affirm that the AD5933 is perfectly suitable for all the applications that this work has studied.

5.3. Spectral Results

The spectral comparison between SFB7 and AD5933+4-AFE per application, showed in section 4.4, present a dispersion at low frequency, between 3 kHz and 6 kHz. This effect could be because the system had not reached the steady state at these frequencies or because at these low frequencies the system is not able to reject the secondary harmonics of the main harmonic. Those problems could be solved just by adding a delay at low frequencies for once or adding a filter in the AFE in the other case.

As it was possible to see on the spectral plots for each application the continuous blue line representing the measurements obtained with the AD5933+4-AFE follow accurately the discontinuous red line representing the measurements taken with the SFB7, in both resistance and reactance. Whereupon the spectroscopy measurements performance exhibited by the AD5933+4-AFE it is possible to conclude that the device will be suitable for the applications under study.

CHAPTER 6

CONCLUSIONS & FUTURE WORK

6.1. Conclusions

After all the results shown in the chapter 4 and discussion in chapter 5, it can be concluded that the combination AD5933+4-AFE is suitable to realize spectroscopy measurements of the EBI applications studied in this master thesis. This result has significant repercussions as in economic terms due to the high integration of AD5933 (I2C interface, DDS, Amplifiers, PGA, Low pass Filter, ADC, DSP and Temperature sensor) as in the electronic instrumentation because it opens up new horizons for the integration of the measurement systems of EBI into portable and even wearable systems.

6.2. Future work

Once the main target of this work has been done, with the aim to solve some problems or to improve the applied method and the system AD5933+4-AFE the next points has brought up:

- The α parameter was chosen arbitrarily and due to it all the models have been affected. Therefore, in order to improve this step in the estimation a study in several subjects should be realized to reach better approximation to α parameter by empiric way.
- The frequency distribution of measurements performed by the SFB7 and AD5933+4-AFE is exponential and linear, respectively. With the goal of improving the comparison between both devices, it will be better to change by software the frequency distribution of the AD5933.
- To use resistors and capacitors with a low tolerance, in order to obtain a lower variability between the models measurements
- To add a larger delay at low frequencies or adding a filter in the AFE to reduce de dispersion at low frequencies.
- Due to the spectral variability of the impedance under study in each application and to make suitable the combination AD5933+4-AFE for many applications, it will be a good improvement to add a differential PGA (Programmable Gain Amplifier) or scalable resistors array.

REFERENCES

[1] S. Grimnes and Ø. G. Martinsen, *Bioimpedance & Bioelectricity Basics*: Academic Press, 2000.

[2] A. Piccoli, B. Rossi, L. Pillon, and G. Bucciante, "A new method for monitoring body fluid variation by bioimpedance analysis: the RXc graph," 1994.

[3] F. Seoane, "Electrical Bioimpedance Cerebral Monitoring: Fundamental Steps towards Clinical Application," in *Signal & Systems*. vol. PhD Göteborg: Chalmers University of Technology, 2007, p. 154.

[4] M. Phillippson, "*Les Lois De La Resistance Electrique Des Tissus Vivants*," *Bull. Acad. roy. Belgique,* 1921.

[5] H. Fricke, "A Mathematical Treatment of the Electrical conductivity of Colloids and Cell Suspensions," *Journal of General Physiology,* pp. 375-383, Jan 4 1924.

[6] K. S. Cole, "Electric impedance of suspensions of spheres," *Journal of General Physiology,* vol. 12, pp. 29-36, 1928.

[7] J. Nyboer, S. Bango, A. Barnett, and R. H. Halsey, "Radiocardiograms: Electrical impedance changes of the heart in relation to electrocardiograms and heart sounds," *J. Clin. Invest.,* vol. 19, p. 773, 1940.

[8] T. Olsson and L. Victorin, "Transthoracic impedance, with special reference to newborn infants and the ratio air-to-fluid in the lungs," *Acta Paediatr Scand Suppl,* vol. 207, p. Suppl 207:1ff, 1970.

[9] R. F. Kushner and D. A. Schoeller, "Estimation of total body water by bioelectrical impedance analysis," *Am J Clin Nutr,* vol. 44, pp. 417-24, Sep 1986.

[10] P. Aberg, I. Nicander, J. Hansson, P. Geladi, U. Holmgren, and S. Ollmar, "Skin cancer identification using multifrequency electrical impedance – A potential screening tool," *IEEE Trans. Bio. Med. Eng.,* vol. 51, pp. 2097-2102, 2004.

[11] H. P. Schwan, "Electrical properties of tissue and cell suspensions," *Adv Biol Med Phys,* vol. 5, pp. 147-209, 1957.

[12] H. Morel and M. Y. Jaffrin, "Total body water measurement: using the multifrequency BIS-Hanai approach with 50 kHz single frequency," in *13th International Conference on Electrical Bioimpedance and the 8th Conference on Electrical Impedance Tomography*, 2007, pp. 799-802.

[13] A. De Lorenzo, A. Andreoli, J. Matthie, and P. Withers, "Predicting body cell mass with bioimpedance by using theoretical methods: a technological review," *J Appl Physiol,* vol. 82, pp. 1542-58, May 1997.

[14] U. Kyle, I. Bosaeus, A. D. De Lorenzo, P. Deurenberg, M. Elia, J. M. Gomez, B. L. Heitmann, L. Kent-Smith, J. Melchior, M. Pirlich, H. Scharfetter, A. M. W. J. Schols, and C. Pichard, "Bioelectrical impedance analysis--part I: review of principles and methods," 2004.

[15] M. Y. Jaffrin and H. Morel, "Body fluid volumes measurements by impedance: A review of bioimpedance spectroscopy (BIS) and bioimpedance analysis (BIA) methods," *Medical Engineering & Physics,* vol. 30, pp. 1257-1269, 2008.

[16] G. B. Forbes, *Human body composition : growth, aging, nutrition, and activity / Gilbert B. Forbes*: Springer-Verlag, 1987.

[17] F. J. Deurenberg P Fau - Schouten and F. J. Schouten, "Loss of total body water and extracellular water assessed by multifrequency impedance."
[18] U. G. Kyle, I. Bosaeus, A. D. De Lorenzo, P. Deurenberg, M. Elia, J. M. Gomez, B. L. Heitmann, L. Kent-Smith, J. C. Melchior, M. Pirlich, H. Scharfetter, A. M. W. J. Schols, and C. Pichard, "Bioelectrical impedance analysis--part I: review of principles and methods," *Clin Nutr*, vol. 23, pp. 1226-43, Oct 2004.
[19] R. Patel, E. L. Peterson, N. Silverman, and B. J. Zarowitz, "Estimation of total body and extracellular water in post-coronary artery bypass graft surgical patients using single and multiple frequency bioimpedance," 1996.
[20] W. Hannan, S. J. Cowen, C. E. Plester, K. C. Fearon, and A. Beau, "Comparison of bio-impedance spectroscopy and multi-frequency bio-impedance analysis for the assessment of extracellular and total body water in surgical patients," 1995.
[21] K. S. Cole, "Permeability and impermeability of cell membranes for ions.," *Quant. Biol.*, vol. 8, pp. 110–122, 1940.
[22] T. Hanai, N. Koizumi, and R. Gotoh, "Dielectric properties of emulsions," *Colloid & Polymer Science*, vol. 184, pp. 143-148, 1962.
[23] P. Nopp, N. Harris, T. Zhao, and B. Brown, "Model for the dielectric properties of human lung tissue against frequency and air content," *Medical and Biological Engineering and Computing*, vol. 35, pp. 695-702, 1997.
[24] L. A. Baker Le Fau - Geddes, H. E. Geddes La Fau - Hoff, C. J. Hoff He Fau - Chaput, and C. J. Chaput, "Physiological factors underlying transthoracic impedance variations in respiration."
[25] L. E. Baker, L. A. Geddes, and H. E. Hoff, "quantitative evaluation of impedance spirometry in man," *The American journal of medical electronics*, 1965.
[26] A. F. Pacela, "Impedance pneumography--a survey of instrumentation techniques."
[27] A. Fein, R. F. Grossman, J. G. Jones, P. C. Goodman, and J. F. Murray, "Evaluation of transthoracic electrical impedance in the diagnosis of pulmonary edema," *Circulation*, 1979.
[28] F. Larsen, L. Mogensen, and B. Tedner, "Transthoracic electrical impedance at 1 and 100 kHz--a means for separating thoracic fluid compartments?," *Clinical Physiology*, 1987.
[29] F. Seoane, J. Ferreira, J. J. Sanchéz, and R. Bragós, "Analog Front-End Enables Electrical Impedance Spectroscopy System On-Chip for Biomedical Applications," *Physiol. Meas.* , vol. 29 pp. S267-S278, 2008.
[30] H. Fricke and S. Morse, "The Electric Resistance and Capacity of Blood for Frequencies Between 800 and 4.5 Million Cycles," *Journal of General Physiology*, vol. 9, pp. 153-67, 1925.
[31] J. Ferreira and J. J. Sanchez, "Electrical Bioimpedance Measurement System for Limb Edema Monitoring," in *School of Engineering*. vol. MSc Borås: University College of Borås, 2007, p. 104.
[32] H. Scharfetter, P. Hartinger, H. Hinghofer-Szalkay, and H. Hutten, "A model of artefacts produced by stray capacitance during whole body or segmental bioimpedance spectroscopy," *Physiological Measurement*, vol. 19, pp. 247-261, 1998.
[33] J. Taylor, *An Introduction to Error Analysis*: University Science Books, 1997.
[34] M. Balleza, N. Calaf, T. Feixas, M. González, D. Antón, P. J. Riu, and P. Casan, "Medición del patrón ventilatorio mediante tomografía por impedancia eléctrica en pacientes con EPOC " *Archivos de bronconeumología*, vol. 45 núm. 07, pp. 320-324, 2009.

[35] M. Balleza, J. Fornos, N. Calaf, T. Feixas, M. González, D. Antón, P. J. Riu, and P. Casan, "Seguimiento del patrón ventilatorio en reposo mediante tomografía por impedancia eléctrica " *Archivos de Bronconeumología,* vol. 43, núm 6, pp. 300-303, 2007.
[36] L. Nescolarde, J. Rosell, and T. Doñate, "Relationship between segmental and whole-body phase angle in peritoneal dialysis patients," *Physiological Measurement,* vol. 29, p. N49, 2008.